Accepted Manuscript

Design, synthesis, in-silico and biological evaluation of novel chalcone derivatives as multi-function agents for the treatment of Alzheimer's disease

Zhipei Sang, Keren Wang, Pengfei Zhang, Jian Shi, Wenmin Liu, Zhenghuai Tan

PII: S0223-5234(19)30642-7

DOI: https://doi.org/10.1016/j.ejmech.2019.07.021

Reference: EJMECH 11518

To appear in: *European Journal of Medicinal Chemistry*

Received Date: 3 April 2019

Revised Date: 3 July 2019

Accepted Date: 6 July 2019

Please cite this article as: Z. Sang, K. Wang, P. Zhang, J. Shi, W. Liu, Z. Tan, Design, synthesis, in-silico and biological evaluation of novel chalcone derivatives as multi-function agents for the treatment of Alzheimer's disease, *European Journal of Medicinal Chemistry* (2019), doi: https://doi.org/10.1016/j.ejmech.2019.07.021.

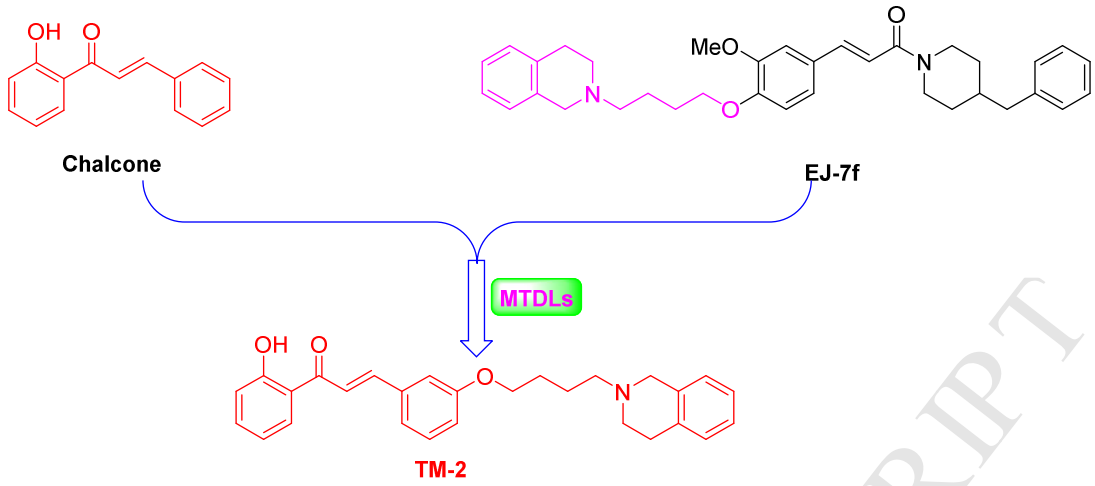

*eq*BChE, IC_{50} = 2.6μM; *ee*AChE, IC_{50} = 16.2μM; MAO-B, IC_{50} = 5.3μM; ORAC = 1.2 eq;
Neuroprotective agent; Metal chelator; Inhibition of self-induced Aβ aggregation: 70.2%
Inhibite Cu^{2+}-induced Aβ aggregation: 80.7%; Disaggregate Cu^{2+}-induced Aβ aggregation: 73.5%
Could cross PAMPA-BBB and conformed to the Lipinski's rule; Presented precognitive effect

Design, synthesis, in-silico and biological evaluation of novel chalcone derivatives as multi-function agents for the treatment of Alzheimer's disease

Zhipei Sang[a,#*], *Keren Wang*[a,#], *Pengfei Zhang*[b], *Jian Shi*[a], *Wenmin Liu*[a,*], *Zhenghuai Tan*[c,*].

[a] *College of Chemistry and Pharmaceutical Engineering, Nanyang Normal University, Nanyang, 473061, China*

[b] *School of Medicine, Henan University Minsheng College, Kaifeng, 475000, China*

[c] *Institute of Traditional Chinese Medicine Pharmacology and Toxicology, Sichuan Academy of Chinese Medicine Sciences, Chengdu, 610041, China*

Abbreviations: AD, Alzheimer's disease; AChEs acetylcholinesterase inhibitors; NMDA, *N*-methyl-D-aspartate; ACh, acetylcholine; AChE, acetylcholinesterase; BuChE, butyrylcholinesterase; Aβ, β-amyloid; ROS, reactive oxygen species; MAO, monoamine oxidase; DA, dopamine; 5-HT, serotonin; NE, noradrenaline; MTDLs, multitarget-directed ligands; *Ee*AChE, *Electrophorus electricus* AChE; *eq*BuChE, *equine serum* BuChE; PDB, Protein Data Bank; *Tc*AChE, *Torpedo californica* AChE; CAS, catalytic active site; PAS, peripheral anionic site; ORAC-FL, Oxygen Radicals Absorbance Capacity by Fluorescence; ThT, thioflavin T; TEM, transmission electron microscopy; MTT, 3-(4,5-dimethylthiazol-2-yl)-2,5-diphenyltetrazolium; PAMPA-BBB, parallel artificial membrane permeation assay of the blood−brain barrier; TPSA, topological polar surface area; HPLC, high-performance liquid chromatography; PBS, phosphate-buffered saline; DTNB, 5,5'-dithiobis-2-nitrobenzoic acid.

#These authors contributed equally.

**Corresponding Author*.

E-mail: sangzhipei@126.com (Zhipei Sang)

E-mail: liuwm1969@163.com (Wenmin Liu)

E-mail: tanzhh616@163.com (Zhenghuai Tan)

Abstract

A series of novel chalcone derivatives was designed, synthesized and evaluated as multifunctional agents for the treatment of AD. Among of these synthesized compounds, compound **TM-2** was a selective BuChE inhibitor (IC_{50} = 2.6 μM) and selective MAO-B inhibitor (IC_{50} = 5.3 μM), which were supported by docking study. Compound **TM-2** also showed good antioxidant activity, and was a selective metal chelator, as well as a neuroprotectant. Moreover, compound **TM-2** could significantly inhibit self-induced and Cu^{2+}-induced A$\beta_{1\text{-}42}$ aggregation with 70.2% and 80.7% inhibition rate, respectively, and could disaggregate Cu^{2+}-induced A$\beta_{1\text{-}42}$ aggregation (73.5%), the further TEM images observed provided rational explanation. Besides, compound **TM-2** displayed good PAMPA-BBB permeability and conformed to the Lipinski's rule of five. Further, compound **TM-2** presented precognitive effect on scopolamine-induced memory impairment in vivo assay. Therefore, compound **TM-2** might be a promising multifunctional hit compound for the treatment of AD, and the further structure optimization are in progress.

Keywords: Alzheimer's disease; chalcone derivatives; Multifunctional agents; BuChE inhibitors; Antioxidant agents; Monoamine oxidase B inhibitor; Aβ aggregation inhibitors; Biometals chelator; Neuroprotective effect; Precognitive effect

1. Introduction

Alzheimer's disease (AD) is a progressive and fatal neurodegenerative disorder affecting 46 million people. It is characterized by the progressive deterioration of various cognitive domains, including a decline in memory and thinking [1]. The current clinical drugs for the treatment of AD include four acetylcholinesterase inhibitors (AChEIs) such as tacrine, donepezil, galantamine and rivastigmine and one *N*-methyl-D-aspartate (NMDA) receptor antagonists, namely memantine. Although these single-target drugs could temporarily delay the progression of cognitive decline in AD, their effects are modest. In addition, AChEIs produce several undesirable side effects, such as gastrointestinal disturbances, bradycardia, and excessive salivation, which are associated with peripheral cholinergic receptors [2]. Up to now, the pathogenesis of AD is still not known, with several competing hypotheses, such as the cholinergic hypothesis, amyloid hypothesis, oxidative stress hypothesis and metal chelation hypothesis, attempting to explain it [3, 4].

According to the "cholinergic hypothesis", cognitive decline in AD is closely related to the level of acetyl choline (ACh) [5, 6]. Normally, ACh can be hydrolyzed by both AChE and BuChE. The recent studies show that AChE plays the major role in the hydrolysis of ACh in the healthy brain, while BuChE takes over the hydrolysis of AChE in the AChE deficient brain. As AD developed, the AChE level in the brain decreases progressively, but BuChE activity increases up to 165% of the normal level [7]. In addition, selective BuChE inhibition is potentially advantageous because it may circumvent the classical cholinergic toxicity that is a common side effect of AChE inhibition [8]. Therefore, BuChE is a promising target for the treatment of the advanced stages of AD.

The production and accumulation of soluble amyloid oligomers of Aβ are a central event in the neuropathology of AD based on the "amyloid hypothesis" [9, 10], as they are thought to be able to initiate the pathogenic cascade, ultimately leading to neuronal loss and dementia. Aβ_{40} and Aβ_{42} are the main isoforms of Aβ peptides, increasing evidences suggest that Aβ_{42} shows more toxic than Aβ_{40}. In addition, Aβ_{42}

could form protofibrils and fibrillar aggregates at lower concentrations. Thus, preventing the formation and aggregation of A$\beta_{1\text{-}42}$ is a potential therapeutic approach for AD.

Oxidative damage is one of the major causes of AD [11], affecting every class of biological macromolecules, such as nucleic acids, proteins, carbohydrates and lipids. It also triggers amyloid plaques and neurofibrillary tangles. Therefore, antioxidant protection is an important way to treat AD. Moreover, transition metals, such as Cu^{2+}, Zn^{2+}, Al^{3+} and Fe^{2+}, could promote Aβ aggregation, and might contribute to the production of reactive oxygen species (ROS) and oxidative stress, implying that these biometals are closely related to several critical aspects of AD [12,13]. So, modulation of these biometals in the brain might be a potential therapeutic strategy against AD.

Monoamine oxidase (MAO), an enzyme of the protein family of flavin-containing amine oxidoreducatases, is responsible for the metabolism of neurotransmitters such as dopamine (DA), serotonin (5-HT), and noradrenaline (NE). There are two types of MAO, hMAO-A and hMAO-B. Studies show that hMAO-A catalyzes the oxidative deamination of serotonin, adrenaline, and noradrenaline, while, hMAO-B preferentially leads to deamination of β-phenethylamine and benzylamine [14]. Recently, the selective MAO-B inhibitor, such as selegiline, has been shown to significantly improve learning and memory deficits in animal models associated with AD and to slow the disease progression in AD patients [15]. So, selective MAO-B inhibitors seem to be an effective treatment of AD.

Due to the complexity of AD and the involvement of multi-systems in its progression, multi-target-directed ligands (MTDLs) strategy is considered to be an effective way to treat this disease [16-18]. These multi-functional agents, simultaneously possessing two or more complementary biological activities, may present an important clinical advance in the future.

Chalcones (α-phenyl-β-benzoylethylene) are prominent secondary-metabolite precursors of flavonoids and isoflavonoids, and could be found widely in plants.

Chalcone and its derivatives are important bioactive molecules with multi biological activities including antioxidant activity, metal chelation property, anti-inflammatory, MAO-B inhibition and neuroprotective properties [19, 20]. In our previous work, the multi-functional agent compound **EJ-7f** showed significantly selective BuChE inhibitory activity, and the *O*-alkylamines fragment was the important pharmacophore group [21]. However, compound **EJ-7f** exhibited weak antioxidant activity, moderate inhibition effect on Aβ aggregation, and compound **EJ-7f** did not show metal chelating ability and hMAO-B inhibitory activity. Therefore, according to the MTDLs drug design strategy, we plan to fuse chalcone and **EJ-7f** to obtain novel chalcone derivatives (**Figure 1**), to test whether these novel molecules possess complementary multi-functional activities.

In this paper, a series of chalcone derivatives were designed and synthesized based on MTDLs. These target compounds were evaluated by ChEs/MAOs inhibition, effect on A$\beta_{1\text{-}42}$ aggregation, antioxidant activity, biometals chelation ability, neuroprotective effect, the ability of cross blood-brain barrier *in vitro* and precognitive effect *in vivo* assay. Besides, docking studies were also performed to provide rational explanation for their biological activities.

<Insert **Figure 1**>

2. Results and discussion

2.1. Chemistry

The synthetic route of target compounds **TM-1~TM-8** was depicted in **Scheme 1** and **Scheme 2**. In the **Scheme 1**, the starting material 3-hydroxybenzaldehyde **1** was treated with excessive amounts of 1,3-dibromopropane (**2a**), 1,4-dibromobutane (**2b**), 1,5-dibromopentane (**2c**) or 1,6-dibromohexane (**2d**), respectively, in the presence of K_2CO_3 in anhydrous acetonitrile at 65 °C to obtain the intermediates **3a-3d**, and then the intermediates **3a-3d** were reacted with cyclic secondary amines **4a** and **4b** to get intermediates **5a~5e**. Finally, the target compounds **TM-1~TM-5** were obtained by

the condensation of intermediates **5a~5e** with 1-hydroxy acetophenone **6** in alcoholic 50% KOH solution.

<Insert **Scheme 1**>

Additionally, as for the synthesis of **TM-6~TM-8**, 2',4'-dihydroxyacetophenone **7** was used as raw material, the key intermediates **9a~9c** were obtained under the same experiments condition described in **Scheme 2**. Finally, benzaldehyde derivatives **10a~10c** were reacted with intermediates **9a~9c** in alcoholic 50% KOH solution to get the target compounds **TM-6~TM-8**.

<Insert **Scheme 2**>

<Insert **Scheme 3**>

Further, as shown in **Scheme 3**, **TM-9** was obtained by the reduction reaction of **TM-2** in the presence of Pd/C and H_2. These target compounds **TM-1~TM-9** have not been reported in the literature. Their structures were confirmed by ^{1}H NMR, ^{13}C NMR and ESI–MS spectroscopy.

2.2. Pharmacology

*2.2.1 Inhibition studies on AChE and BuChE***.** The inhibitory activities of target compounds **TM-1~TM-9** against *ee*AChE (from *electric eel*) and *eq*BuChE (from *equine serum*) were evaluated using the modified Ellman's method [22, 23]. Chalcone and donepezil were tested as the positive control. The results were listed in **Table 1**, expressed as IC_{50} values. As expected, the target compounds **TM-1~TM-9** showed moderate to good inhibitory activity against AChE and BuChE compared with chalcone, implying that introduction of *O*-alkylamines fragment could increase the AChE/BuChE inhibitory activity, which was consistent with our design strategy. According to the screening data in **Table 1**, the terminal groups NR_1R_2 and methylene chain length of side chain significantly affected the inhibitory activities of *eq*BuChE. Firstly, the BuChE inhibitory activity presented positive trend as the methylene chain length increased, and the optimal methylene chain length was 4, such as **TM-1** (IC_{50} =

11.2 μM) > **TM-2** (IC_{50} = 2.6 μM) < **TM-3** (IC_{50} = 3.7 μM) < **TM-4** (IC_{50} = 4.1 μM). Replacing the 1,2,3,4-tetrahydroisoquinoline of **TM-2** with 4-benzylpiperidine to obtain compound **TM-5**, the BuChE inhibitory activity decreased to 4.9 μM, it showed that 1,2,3,4-tetrahydroisoquinoline fragment contributed to BuChE inhibition. Secondly, in order to further explore the structure-activity relationship, we changed the position of side chain of **TM-1** (IC_{50} = 11.2 μM) to get compound **TM-6**, the BuChE inhibitory activity decreased to 13.4 μM, and then changing the position of side chain of **TM-2** to get compound **TM-7**, the BuChE inhibitory activity increased to 5.2 μM, but it showed good AChE inhibitory activity with IC_{50} value of 8.3 μM. Moreover, changing the position of side chain of **TM-4** to obtain compound **TM-8**, which was a selective AChE inhibitor (IC_{50} = 6.6 μM) and displayed moderate BuChE inhibitory potency (IC_{50} = 10.4 μM). According to the phenomenon observed, changing the position of side chain could decrease the BuChE inhibitory activity, but increased the AChE inhibitory potency. Besides, the electron-donating groups, such as OCH_3 in **TM-7** and $N(CH_3)_2$ in **TM-8**, were beneficial to AChE/BuChE inhibition, while the electron-withdrawing group (such as F in **TM-6**) decreased the BuChE inhibitory activity. Thus, compound **TM-2** exhibited the best BuChE inhibitory activity with IC_{50} value of 2.6 μM, and compound **TM-8** indicated the best AChE inhibitory potency (IC_{50} = 6.6 μM). More interestingly, when compound **TM-2** was reduced to **TM-9** in the presence of Pd/C and H_2, the BuChE inhibitory activity increased to 0.64 μM, but **TM-9** showed weak AChE inhibitory activity with IC_{50} value of 23.1 μM, suggesting that the reduction reaction of olefinic bond contributed to BuChE inhibitory activity.

<Insert **Table 1**>

*2.2.2 Molecular modeling studies of **TM-2**.* According to the above results, compound **TM-2** would be the optimal compound to further study. The further computational study was performed to explore possible binding mechanism of AChE and BuChE for compound **TM-2** using the docking program, AutoDock 4.2 package with Discovery Studio 2.5, based on the X-ray crystal structure of AChE (PDB code: 1EVE) and

BuChE (PDB code: 4tpk) [21, 24]. The results indicated that **TM-2** could occupy the entire AChE enzymatic catalytic active site (CAS), the mid-gorge sites and the peripheral anionic site (PAS) (**Figure 2**). The hydroxyl group and carbonyl group of **TM-2** formed one intramolecular hydrogen bonding interaction, and the hydroxyl interacted with Phe331 via intermolecular hydrogen bonding, moreover, the benzene ring of chalcone skeleton interacted with key amino acid Tyr334 via σ-π interaction. Meanwhile, hydrophobic interactions could be observed between the ligand and amino acid residues Asp72, Trp84, Gly118, Gly123, Tyr121, Phe290, Phe288, Tyr334, and Phe331.

<Insert **Figure 2**>

In the **TM-2**-BuChE complex, we found that compound **TM-2** interacted with BuChE via multiple sites (**Figure 3**), the hydroxyl group and carbonyl of chalcone skeleton interacted via intramolecular hydrogen bonding, and further the hydroxyl interacted with Ser287 via intermolecular hydrogen bonding. In addition, the benzene ring of 1,2,3,4-tetrahydroisoquinoline interacted with the benzene ring of chalcone skeleton via π-π interaction, and the benzene ring of 1,2,3,4-tetrahydroisoquinoline interacted with key amino acid Tyr332 via π-π interaction, and one intermolecular hydrogen bonding was observed between ligand **TM-2** and key amino acid Trp82. Besides, hydrophobic interactions could be observed between the ligand and important amino acid residues Trp82, Phe329, Tyr332, Ser287, Trp231 and His438. Therefore, the phenomenon observed might provide the rational explanation for the highly selective BuChE inhibition of **TM-2**.

<Insert **Figure 3**>

*2.2.3 BuChE reversibility of inhibition by **TM-2**.* The recovery of *eq*BuChE inhibitory activities after dilution with time monitoring were tested to evaluate the *eq*BChE reversibility inhibition by **TM-2** [25]. As shown in **Figure 4A**, the 0.1 × IC_{50} of standard donepezil increased *eq*BChE activity to 9.4% compared with control, that implying partial recovery of the *eq*BChE from donepezil. While the 0.1 × IC_{50} of standard rivastigmine increased *eq*BChE activity to -0.7%, indicating no recovery of

the *eq*BChE from rivastigmie. In addition, under the same condition, the 0.1 × IC_{50} of **TM-2** *eq*BChE activity to 8.2%, as similar with donepezil. Furthermore, according to the screening data in **Figure 4B**, the *eq*BChE activity restored to 126.8% with 0.1× IC_{50} donepezil at 240 min, and the *eq*BChE activity of 0.1× IC_{50} rivastigmine gradually increased to 73.2% at 240 min. As expected, and the *eq*BChE activity of 0.1× IC_{50} **TM-2** increased to 103.5% at 240 min, similar with donepezil. So, the observed phenomenon revealed that compound TM-2 was a reversible BuChE inhibitor.

<Insert **Figure 4**>

2.2.4 Inhibition of MAOs in vitro. As shown in **Table 1**, the MAO-A and MAO-B (recombinant human enzyme) inhibitory activities of target compounds **TM-1~TM-9** were determined, iproniazid and rasagiline were also tested as referenced compounds [26]. The results showed that all the target compounds indicated selective MAO-B inhibitory activities, which contributed to the treatment of AD. Among of these target compounds, compound **TM-3** showed the best MAO-B inhibitory activity with IC_{50} value of 4.8 μM. According to the structure-active-relationship, the MAO-B inhibitory activity improved as methylene chain increased, while the optimal methylene chain was 5, such as **TM-1** (IC_{50} = 10.7 μM) > **TM-2** (IC_{50} = 5.3 μM) > **TM-3** (IC_{50} = 4.8 μM) < **TM-4** (IC_{50} = 6.7 μM), in addition, the side chain terminal NR_1R_2 fragment did not display obvious effect on MAO-B inhibitory activity, such as **TM-5** (IC_{50} = 6.4 μM) *vs* **TM-2**. Moreover, the position of side chain also affected the inhibitory activity, compounds **TM-6**~**TM-8** was obtained by changing the position of *O*-alkylamines, the results showed that compounds **TM-7** and **TM-8** with electron-donating groups indicated better MAO-B inhibitory potency than compound **TM-6** with electron-withdrawing group. Further, the ethylenic bond of compound **TM-2** was reduced to **TM-9**, the MAO-B inhibitory activity sharply decreased to 26.7 μM, and MAO-A inhibitory activity did not show obvious change, suggesting that the α,β-unsaturated ketone fragment was conducive to MAO-B inhibitory activity.

2.2.5 Molecular modeling study of MAO-B. To further study the binding mode of

TM-2 with MAO-B, molecular docking study based on the X-ray crystal structures of human MAO-B (PDB code: 2V60) was performed [26]. As shown in **Figure 5**, the 2-hydroxy acetophenone moiety of **TM-2** was located in the well-known binding pocket of *hu*MAO-B, in close proximity to the enzymatic cofactor FAD, and formed one intermolecular hydrogen bonding interaction. Moreover, the benzene ring of chalcone skeleton interacted with Tyr398 via π-π interaction, and the benzene ring of 1,2,3,4-tetrahydroisoquinoline interacted with Ile316 via σ-π interaction. Meanwhile, hydrophobic interactions could be observed between the ligand and residues Ile316, Phe168, Ile199, Pro102, Phe103, Tyr326, Phe343, Tyr435 and Leu88. Thus, the phenomenon observed could explain why **TM-2** could decrease the MAO-B inhibitory activity.

<Insert **Figure 5**>

2.2.6 Antioxidant Activity in Vitro. The antioxidant activities of the target compounds **TM-1~TM-9** were tested by the ORAC-FL method (Oxygen Radicals Absorbance Capacity by Fluorescence) [27, 28]. The vitamin E analogue Trolox was used as a standard. According to the screening data in **Table 1**, all the compounds exhibited good ORAC-FL values of 0.92−1.6 Trolox equivalents. The terminal groups NR_1R_2 and methylene chain length of side chain showed no obvious influence on the antioxidant activity, such as **TM-1~TM-5**. When changing the position of side chain, the data showed that the compounds with electron-donating groups (**TM-7** and **TM-8**) displayed better antioxidant activity than compound **TM-6** with electron-withdrawing group. It might be that the electron-donating groups help antioxidant activity. In addition, compound **TM-9** showed good antioxidant activity with ORAC value of 1.4 eq.

2.2.7 Inhibition of Self-induced Aβ_{1-42} Aggregation. The inhibitory activities of the target compounds against self-induced Aβ_{1-42} aggregation were evaluated using a thioflavin T (ThT) fluorescence assay [29]. Curcumin was used as reference compound. As summarized in **Table 2**, all the target compounds **TM-1~TM-8** displayed more inhibition of self-induced A$\beta_{\mathbf{1-42}}$ aggregation than curcumin (43.1% at

25 μM). Taken together, the *O*-alkylamines side chain showed no meaningful impact on self-induced Aβ_{1-42} aggregation inhibition. While, changing the *O*-alkylamines side chain of **TM-1~TM-5** to obtain **TM-6~TM-8**, the inhibitory activity remarkably improved, and further the electron-donating groups (**TM-7** and **TM-8**) in chalcone skeleton displayed better inhibitory activity than compound **TM-6** with electron-withdrawing group in chalcone skeleton, especially, compound **TM-8** with dimethylamino group exhibited the best inhibitory activity with 97.5% inhibition rate at 25 μM. It might be that the electron-donating groups served as an important role in the inhibition of self-induced Aβ_{1-42} aggregation.

<Insert **Table 2**>

2.2.8 Molecular modeling studies of A*β*. To further explore the binding mode of the compound **TM-2** with A*β* (PDB: 1BA4), a molecular docking experiment was performed [30]. As shown in **Figure 6**, compound **TM-2** was locked at the C-terminal hydrophobic area of A*β*. The hydroxyl group and carbonyl group of chalcone skeleton formed one intramolecular hydrogen bonding, and further the carbonyl interacted with Asp1 via intermolecular hydrogen bonding. In addition, the benzene ring of chalcone skeleton interacted with Lys 16 *via* positive ion-π interaction, and the methylene chain interacted with Phe19 via two σ-π interactions. Moreover, compound **TM-2** formed the hydrophobic interactions with the residues ASP1, PHE20, LYS28, ASN27 and ILE31. These interactions might be favorable for the binding of A*β* and compound **TM-2**.

<Insert **Figure 6**>

*2.2.9 Metal-chelating properties of compound **TM-2**.* The ability of compound **TM-2** to chelate biometals such as Cu^{2+}, Zn^{2+}, Al^{3+}, Fe^{2+}, Cu^{+} and Fe^{3+} was studied by UV-vis spectrometry [31]. As shown in **Figure 7**, when compound TM-2 was treated with $CuCl_2$ and $AlCl_3$, the maximum absorption wavelength shifted from 361 nm to 418 nm and 426 nm, respectively, indicating the formation of **TM-2**-Cu^{2+} and **TM-2**-Al^{3+}complex. Conversely, the maximum absorption exhibited no significant

shift after adding Zn^{2+}, Fe^{2+}, Cu^{+} and Fe^{3+}. These results indicated that the compound **TM-2** was a selective metal chelator.

<Insert **Figure 7**>

The stoichiometry of the **TM-2**-Cu^{2+} complex was determined using molar ratio method by preparing solutions of compound **TM-2** with increasing amounts of $CuCl_2$. According to the **Figure 8**, the absorbance linearly increased at first and then tended to be stable at 426 nm. The two straight lines intersected at a mole fraction of 1.01, revealing a 1:1 stoichiometry for complex **TM-2**-Cu^{2+}.

<Insert **Figure 8**>

2.2.10 Effects on Cu^{2+}-induced Aβ_{1-42} aggregation and disaggregation. Thioflavin T (ThT) binding assay was used to test inhibition and disaggregation effect of **TM-2** on Cu^{2+}-induced Aβ_{1-42} aggregation [32, 33]. As shown in **Table 2**, compound **TM-2** could inhibit Cu^{2+}-induced Aβ_{1-42} aggregation with 80.7% inhibition rate, which was better than that of curcumin (76.5%). And transmission electron microscopy (TEM) supported the data, **Figure 9B** illustrated that the sample of Aβ_{1-42} aggregated into amyloid fibrils after adding 25 μM Cu^{2+} for 24 h incubation, while only small bulk aggregations were observed in the sample of Aβ_{1-42} in the presence of **TM-2**. In addition, compound **TM-2** remarkably disaggregated Cu^{2+}-induced Aβ_{1-42} aggregation (73.5% at 25 μM), which was supported by TEM in **Figure 9D**. Thus, both the data and TEM revealed that **TM-2** could inhibit and disaggregate Cu^{2+}-induced Aβ_{1-42} aggregation fibrils.

<Insert **Figure 9**>

2.2.11 Neuroprotective effects on H_2O_2-induced PC12 cell injury. The 3-(4,5-dimethylthiazol-2-yl)-2,5- diphenyltetrazolium (MTT) assay was performed to test the protective effects of **TM-2** against H_2O_2–induced injury [34]. As shown in **Figure 10A**, **TM-2** had a wide therapeutic safety range. In addition, cell viability was

sharply declined to 51.3 % ($p < 0.01$ *vs* control) after 100 μM H_2O_2 exposure in **Figure 10B**, while compound **TM-2** showed protective effects in a dose-dependent manner against H_2O_2-induced PC12 cell injury. At concentrations of 10.0 μM, the cell viability of compound **TM-2** was 82.6%, exhibiting significantly neuroprotective effects, and the cell viability decreased to 61.9% as the concentration reduced to 1.0 μM. Therefore, the results revealed that compound **TM-2** possessed potent neuroprotective effect on H_2O_2–induced cell injury.

<Insert **Figure 10**>

2.2.12 In vitro blood−brain barrier permeation assay. The parallel artificial membrane permeation assay of the blood−brain barrier (PAMPA-BBB) was performed to evaluate the BBB permeability of target compounds **TM-1~TM-9** [35, 36]. 11 commercial drugs were selected to validate the assay (**Table 3**), a good linear correlation was produced, $P_e(exp) = 0.9163P_e(bibl.) - 0.2247$ ($R^2 = 0.9558$) **(Figure 11**). From the expression and considering the limit established by Di *et al*., compounds with permeability above 3.44×10^{-6} cm/s were considered to cross the blood−brain barrier (**Table 4**). According to the measured permeability in **Table 5**, all the target compounds could cross the BBB *in vitro*.

<Insert **Table 3**>

<Insert **Figure 11**>

<Insert **Table 4**>

<Insert **Table 5**>

2.2.13 Theoretical evaluation of ADME properties. To evaluate the druglike properties of chalcone derivatives **TM-1~TM-9**, we adopted the Molinspiration property program to calculate the items including milog *P*, pKa, topological polar surface area (TPSA), the number of hydrogen-bond acceptors, and the number of hydrogen-bond

donors [37]. From the data listed in **Table 6,** we determined that compound **TM-2** abided by the Lipinski's rule of five, acting as a promising drug candidate.

<Insert **Table 6**>

2.2.14 In vivo assay

Acute Toxicity. The acute toxicity of **TM-2** was assessed in Kunming mice at doses of 250, 500 and 1000 mg/kg (n = 10 per group). After oral administration of compound **TM-2**, mice were observed continuously for the first 4 h through 14 days for any abnormal behavior and mortality changes. The results exhibited that the animals treated with compound **TM-2** did not show any acute toxicity or mortality immediately.

Effect on scopolamine-induced memory impairment. The step-down passive avoidance task was performed to further assess whether **TM-2** could improve scopolamine-induced memory impairment [38, 39]. As shown in **Figure 12**, treatment with scopolamine alone, the step-down latency time sharply decreased to 70.4 sec ($p < 0.01$) compared with normal group (159.7 sec). While after treatment with donepezil (5 mg/kg), the latency time significantly increased to 151.7 sec ($p < 0.01$) compared with scopolamine group, thus implying that the model worked well. In addition, treatment with compound **TM-2** (16.8, 5.6 and 1.9 mg/kg) increased the latency time in a dose-dependent manner, and the high dose group (16.8 mg/kg) presented the longest latency time (126.4 sec., $p < 0.05$) of the three dose groups, but the high dose (16.8 mg/kg) of compound **TM-2** showed lower latency time than the drug control group with donepezil (5 mg/kg, 151.7 sec). These results showed that compound **TM-2** could improve scopolamine-induced memory impairment, and the optimal dose was 16.8 mg/kg.

<Insert **Figure 12**>

3. Conclusion

In summary, a series of chalcone derivatives was designed and synthesized as multifunctional agents for the treatment of AD. All the target compounds were evaluated by ChEs/MAOs inhibitory activities, antioxidant activity, effect on A$\beta_{1\text{-}42}$ aggregation. Among of these synthetic compounds, compound **TM-2** indicated the best BuChE inhibitory activity with IC_{50} value of 2.6 μM, and showed selective MAO-B inhibitory activity (IC_{50} = 5.3 μM), which were supported by molecular docking study. **TM-2** was also an antioxidant and could significantly inhibit self-induced A$\beta_{1\text{-}42}$ aggregation (70.2%). In addition, compound **TM-2** was a selective metal chelator, and could inhibit (80.7%) and disaggregate (73.5%) Cu^{2+}-induced A$\beta_{1\text{-}42}$ aggregation. Moreover, **TM-2** acted as a neuroprotectant and could cross the blood-brain barrier (BBB) *in vitro*, as well as abidance by the Lipinski's rule of five. Further, compound **TM-2** presented precognitive effect on scopolamine-induced memory impairment. Therefore, compound **TM-2** might be a promising multifunctional hit compound for the treatment of AD.

4. Experiment section

4.1. Chemistry

All materials were obtained from commercial suppliers and used without further purification. ^{1}H NMR and ^{13}C NMR spectra were recorded using a Bruker 400 NMR spectrometer. Mass spectra were recorded on Agilent-6210 TOF LC-MS Spectrometer. The purity of compounds was determined by high-performance liquid chromatography (HPLC) analysis to be over 96%. HPLC analysis was carried out on a Shimadzu LC-10Avp plus system with the use of a Kromasil C_{18} column (4.6 mm × 250 mm, 5um). All the final compounds were obtained by column chromatography.

*4.1.1. General procedures for the synthesis of intermediates **3a-3d** and **8a-8c**.* The appropriate dibromoalkane derivative **2a-2d** (25 mmol) were added to a mixture of the starting material 3-hydroxybenzaldehyde (**1**) or 2,4-dihydroxyacetophenone (**7**) (10.0 mmol), and the mixture was heated at 65℃ for 8-12h in the presence of anhydrous K_2CO_3 (12.0 mmol) in 30 mL CH_3CN. The reaction was detected by TLC. The solvent was evaporated under reduced pressure after complete reaction. The

residue was resolved with water (100 mL) and was extracted with CH_2Cl_2 (50 mL × 3). The combined solvents were treated with saturated aqueous NaCl, dried over Na_2SO_4, and filtered. The organic phase was evaporated to obtain crude product, which was purified on a silica gel chromatography using petroleum ether/acetone (30:1) as eluent to give the intermediates **3a-3d** and **8a-8c**.

4.1.1.1 3-(3-bromopropoxy)benzaldehyde ***(3a)***. Colorless oil, 65.7% yield. ^{1}H NMR (400 MHz, $CDCl_3$) δ 9.86 (s, 1H, CHO), 7.33 (d, *J* = 5.6 Hz, 2H, 2 × Ar-H), 7.28 (s, 1H, Ar-H), 7.09-7.05 (m, 1H, Ar-H), 3.93 (t, *J* = 6.4 Hz, 2H, OCH_2), 1.75 (t, *J* = 6.0 Hz, 2H, $BrCH_2$), 1.47-1.43 (m, 2H, CH_2).

4.1.1.2 3-(4-bromobutoxy)benzaldehyde ***(3b).*** Colorless oil, 70.2% yield. ^{1}H NMR (400 MHz, $CDCl_3$) δ 9.89 (s, 1H, CHO), 7.38-7.30 (m, 2H, 2 × Ar-H), 7.30-7.31 (m, 1H, Ar-H), 7.11-7.07 (m, 1H, Ar-H), 3.98 (t, *J* = 5.6 Hz, OCH_2), 3.42 (t, *J* = 5.6 Hz, $BrCH_2$), 2.04-1.97 (m, 2H, CH_2), 1.93-1.86 (m, 2H, CH_2).

4.1.1.3 3-((6-bromohexyl)oxy)benzaldehyde ***(3d).*** Colorless oil, 53.9% yield. ^{1}H NMR (400 MHz, $CDCl_3$) δ9.97 (s, 1H, CHO), 7.45-7.43 (m, 2H, 2 × Ar-H), 7.38 (d, *J* = 2.0 Hz, 1H, Ar-H), 7.19-7.15 (m, 1H, Ar-H), 4.02 (t, *J* = 6.4 Hz, 2H, OCH_2), 3.43 (t, *J* = 6.8Hz, 2H, BrCH2), 1.93-1.86 (m, 2H, CH_2), 1.85-1.79 (m, 2H, CH_2), 1.56-1.49 (m, 4H, 2 × CH_2).

4.1.1.4 1-(4-(3-bromopropoxy)-2-hydroxyphenyl)ethan-1-one ***(8a).*** Colorless oil, 78.4% yield. ^{1}H NMR (400 MHz, $CDCl_3$) δ 12.64 (s, 1H, OH), 7.50 (d, *J* = 8.8 Hz, 1H, Ar-H), 6.31 (d, *J* = 9.2 Hz, 1H, Ar-H), 6.28 (s, 1H, Ar-H), 4.00 (t, *J* = 5.6 Hz, 2H, OCH_2), 3.47 (t, J = 6.0 Hz, 2H, $BrCH_2$), 2.42 (s, 3H, CH_3), 2.25-2.17 (m, 2H, CH_2).

4.1.1.5 1-(4-(4-bromobutoxy)-2-hydroxyphenyl)ethan-1-one ***(8b).*** Colorless oil, 80.5% yield. ^{1}H NMR (400 MHz, $CDCl_3$) δ 12.75 (s, 1H, OH), 7.64 (d, J = 8.8 Hz, 1H, Ar-H), 6.44 (dd, J_1 = 6.8 Hz, J_2 = 2.0 Hz, 1H, Ar-H), 6.41 (d, J = 2.0 Hz, 1H, Ar-H), 4.04 (t, J = 6.0 Hz, 2H, OCH_2), 3.50 (t, J = 6.4 Hz, 2H, $BrCH_2$), 2.57 (s, 3H, CH_3), 2.11-2.04 (m, 2H, CH_2), 2.01-1.94 (m, 2H, CH_2).

4.1.1.6 1-(4-((6-bromohexyl)oxy)-2-hydroxyphenyl)ethan-1-one ***(8c).*** Colorless oil,

68.5% yield. ^{1}H NMR (400 MHz, $CDCl_3$) δ ^{1}H NMR 12.73 (s, 1H, OH), 7.61 (d, J = 8.8 Hz, 1H, Ar-H), 6.42 (d, J = 9.2Hz, 1H, Ar-H), 6.38 (s, 1H, Ar-H), 3.99 (t, J = 6.0 Hz, 2H, OCH_2), 3.42 (t, J = 6.4 Hz, 2H, $BrCH_2$), 2.54 (s, 3H, CH_3), 1.91-1.84 (m, 2H, CH_2), 1.83-1.76 (m, 2H, CH_2), 1.52-1.45 (m, 4H, 2 × CH_2).

*4.1.2. General procedures for the synthesis of intermediates **5a-5e** and **9a-9c**.*

A mixture of the intermediates **3a-3d** (3 mmol) or **8a-8c,** anhydrous K_2CO_3 (4.0 mmol) and corresponding secondary amine NR_1R_2 **4a-4b** (3.5 mmol) was heated at 65 °C in CH_3CN (15 ml). The reaction was treated referenced the detail of *4.1.1*. The residue was purified on a silica gel chromatography using mixtures of petroleum/acetone (15: 1) as eluent to obtain compounds **5a-5e** and **9a-9c**.

*4.1.2.1 3-(4-(3,4-dihydroisoquinolin-2(1H)-yl)butoxy)benzaldehyde (**5b**).* Colorless oil, 85.9% yield. ^{1}H NMR (400 MHz, $CDCl_3$) δ 9.96 (s, 1H, CHO), 7.44-7.42(m, 2H, 2 × Ar-H), 7.38 (s, 1H, Ar-H), 7.19-7.15 (m, 1H, Ar-H), 7.13-7.08 (m, 3H, 3 × Ar-H), 7.03-7.01 (m, 1H, Ar-H), 4.07 (t, *J* = 6.0 Hz, OCH_2), 3.67 (s, 2H, $phCH_2$), 2.92 (t, *J* = 5.6 Hz, $phCH_2$), 2.77 (t, *J* = 5.6 Hz, $phCH_2$), 2.61 (t, *J* = 6.8 Hz, $phCH_2$), 1.91-1.84 (m, 2H, CH_2), 1.83-1.78 (m, 2H, CH_2).

*4.1.2.2 3-((6-(3,4-dihydroisoquinolin-2(1H)-yl)hexyl)oxy)benzaldehyde (**5d**).* Colorless oil, 81.6% yield. ^{1}H NMR (400 MHz, $CDCl_3$) δ 9.91 (s, 1H, CHO), 7.40-7.36 (m, 2H, 2 × Ar-H), 7.35 (s, 1H, Ar-H), 7.15-7.11 (m, 1H, Ar-H), 7.09-7.04 (m, 2H, 2 × Ar-H), 6.99-6.97 (m, 1H, Ar-H), 3.96 (t, J = 6.4 Hz, 2H, OCH_2), 3.59 (s, 2H, $phCH_2$), 2.87 (t, J = 6.0 Hz, 2H, NCH_2), 2.68 (t, J = 6.0 Hz, 2H, NCH_2), 2.48 (t, J = 7.6 Hz, 2H, NCH_2), 1.83-1.76 (m, 2H, CH_2), 1.65-1.58 (m, 2H, CH_2), 1.53-1.46 (m, 2H, CH_2), 1.44-1.39 (m, 2H, CH_2).

*4.1.2.3 3-(4-(4-benzylpiperidin-1-yl)butoxy)benzaldehyde (**5e**).* Colorless oil, 88.3% yield. ^{1}H NMR (400 MHz, $CDCl_3$) δ 9.95 (s, 1H, CHO), 7.43-7.41 (m, 2H, 2 × Ar-H), 7.36 (s, 1H, Ar-H), 7.27 (t, J = 7.2 Hz, 2H, 2 × Ar-H), 7.18 (t, J = 7.6 Hz, 1H, Ar-H), 7.14 (t, J = 7.6 Hz, 3H, 3 × Ar-H), 4.02 (t, J = 4.0 Hz, 2H, 2 × Ar-H), 3.03 (d, J = 11.2 Hz, 2H, $phCH_2$), 2.54 (d, J = 7.2 Hz, 2H, NCH_2), 2.48 (t, J = 7.6 Hz, 2H, NCH_2), 2.00 (t, J = 11.2 Hz, 2H, NCH_2), 1.83-1.74 (m, 4H, 2 × CH_2), 1.67 (d, J = 12.8 Hz, 2H, CH_2), 1.59-1.53 (m, 1H, CH), 1.44 (t, J = 11.6 Hz, 2H, CH_2).

4.1.2.4

*1-(4-(3-(3,4-dihydroisoquinolin-2(1H)-yl)propoxy)-2-hydroxyphenyl)ethan-1-one (**9a**).* Colorless oil, 87.2% yield. ^{1}H NMR (400 MHz, $CDCl_3$) δ 12.73 (s, 1H, OH), 7.62 (d, J = 8.8 Hz, 1H, Ar-H), 7.14-7.08 (m, 3H, 3 × Ar-H), 7.03-7.01 (m, 1H, Ar-H), 6.44 (dd, J_1 = 6.4 Hz, J_2 = 2.4 Hz, 1H, Ar-H), 6.42 (d, J = 2.4 Hz, 1H, Ar-H), 4.11 (t, J = 6.4 Hz, 2H, OCH_2), 3.66 (s, 2H, $phCH_2$), 2.92 (d, J = 5.6 Hz, 2H, $phCH_2$), 2.76 (d, J = 6.0 Hz, 2H, NCH_2), 2.69 (t, J = 7.2 Hz, 2H, NCH_2), 2.55 (s, 3H, $COCH_3$), 2.12-2.05 (m, 2H, CH_2).`

4.1.2.5

*1-(4-(4-(3,4-dihydroisoquinolin-2(1H)-yl)butoxy)-2-hydroxyphenyl)ethan-1-one (**9b**).* Colorless oil, 80.9% yield. ^{1}H NMR (400 MHz, $CDCl_3$) δ 12.75 (s, 1H, OH), 7.60 (d, J = 9.2 Hz, 1H, Ar-H), 7.13-7.08 (m, 3H, 3 × Ar-H), 7.02-7.00 (m, 1H, Ar-H), 6.43 (dd, J1 = 6.4 Hz, J2 = 2.4 Hz, 1H, Ar-H), 6.39 (d, J = 2.4 Hz, 1H, Ar-H), 4.03 (t, J = 6.0 Hz, 2H, OCH_2), 3.64 (s, 2H, $phCH_2$), 2.91 (t, J = 6.0 Hz, 2H, NCH_2), 2.74 (t, J = 6.0 Hz, 2H, NCH_2), 2.58 (t, J = 7.6 Hz, 2H, NCH_2), 2.53 (s, 3H, $COCH_3$), 1.90-1.80 (m, 2H, CH_2), 1.77-1.73 (m, 2H, CH_2).

4.1.2.6

*1-(4-((6-(3,4-dihydroisoquinolin-2(1H)-yl)hexyl)oxy)-2-hydroxyphenyl)ethan-1-one (**9c**).* Colorless oil, 76.9% yield. ^{1}H NMR (400 MHz, $CDCl_3$) δ 12.76 (s, 1H, OH), 7.61 (d, J = 8.8 Hz, 1H, Ar-H), 7.13-7.08 (m, 3H, 3 × Ar-H), 7.02-7.00 (m, 1H, Ar-H), 6.42 (dd, J_1 = 6.4 Hz, J_2 = 2.4 Hz, 1H, Ar-H), 6.40 (d, J = 2.4 Hz, 1H, Ar-H), 3.99 (t, J = 6.4 Hz, 2H, OCH_2), 3.62 (s, 2H, $phCH_2$), 2.90 (t, J = 5.6 Hz, 2H, NCH_2), 2.73 (t, J = 6.0 Hz, 2H, NCH_2), 2.51 (t, J = 7.6 Hz, 2H, NCH_2), 1.83-1.77 (m, 2H, CH_2), 1.65-1.59 (m, 2H, CH_2), 1.52-1.45 (m, 2H, CH_2), 1.43-1.39 (m, 2H, CH_2).

*4.1.3. General procedure for the synthesis of compounds **TM-1~TM-8**.*

A mixture of benzaldehyde derivatives **5a-5e**, **10a**, **10b** and **10c** (5.0 mmol) with the corresponding acetophenone derivatives **6** and **9a-9c** (5.5 mmol) was added slowly to an amount of 30% aqueous KOH (20 mmol) solution in EtOH (7 mL). The mixture was stirred for 72 h at room temperature, and then poured into ice-cold water. Acidified with 10% HCl, and was extracted with CH_2Cl_2 (50 mL × 3), the organic phase was evaporated under reduced pressure. The residue was purified using mixtures of

CH_2Cl_2/acetone (30:1) as eluent on a silica gel chromatography to obtain the products **TM-1~TM-8**.

*(E)-3-(3-(3-(3,4-dihydroisoquinolin-2(1H)-yl)propoxy)phenyl)-1-(2-hydroxyphenyl)prop-2-en-1-one (**TM-1**).*Yellow oil, 46.8% yield, 97.8% HPLC purity. ^{1}H NMR (400 MHz, $CDCl_3$) δ 12.81 (s, 1H, OH), 8.08 (d, J = 7.2 Hz, 1H, Ar-H), 7.94 (d, J = 7.6 Hz, 1H, Ar-H), 7.87 (d, J = 15.6 Hz, CH=CH), 7.64 (d, J = 15.6 Hz, 1H, CH=CH), 7.50 (t, J = 8.0 Hz, 1H, Ar-H), 7.41 (t, J = 7.6 Hz, 1H, Ar-H), 7.33 (t, J = 8.0 Hz, 2H, 2 × Ar-H), 7.24 (d, J = 7.2 Hz, 1H, Ar-H), 7.18 (d, J = 8.0 Hz, 2H, 2 × Ar-H), 7.03 (d, J = 8.0 Hz, 1H, Ar-H), 6.96 (q, J = 7.6 Hz, 2H, 2 × Ar-H), 4.07 (t, J = 5.2 Hz, 2H, OCH_2), 3.67 (s, 2H, phCH_2), 3.59 (t, J = 5.6 Hz, 2H, phCH_2), 3.00 (t, J = 6.0 Hz, 2H, NCH_2), 1.89-1.86 (m, 4H, 2 × CH_2). ^{13}C NMR (100 MHz, $CDCl_3$) 193.8, 163.6, 159.4, 145.4, 137.9, 136.4, 136.0, 131.6, 130.0, 129.8, 129.5, 128.3, 127.1, 126.8, 121.5, 120.4, 120.0, 118.9, 118.6, 117.1, 114.2, 67.6, 46.9, 46.1, 28.2, 26.6, 24.4. MS (ESI) m/z: 414.2 $[M + H]^+$

*(E)-3-(3-(4-(3,4-dihydroisoquinolin-2(1H)-yl)butoxy)phenyl)-1-(2-hydroxyphenyl)prop-2-en-1-one (**TM-2**).* Yellow oil, 50.7% yield, 98.5% HPLC purity. ^{1}H NMR (400 MHz, $CDCl_3$) δ 12.80 (s, 1H, OH), 7.87 (d, J = 7.6 Hz, 1H, Ar-H), 7.75 (d, J = 15.2 Hz, 1H, CH=CH), 7.56 (d, J = 15.2 Hz, 1H, CH=CH), 7.39 (t, J = 8.0 Hz, 1H, Ar-H), 7.23 (t, J = 8.0 Hz, 1H, Ar-H), 7.20-7.13 (m, 1H, Ar-H), 7.09-7.06 (m, 3H, 3 × Ar-H), 7.04 (t, J = 7.2 Hz, 1H, Ar-H), 6.98-6.90 (m, 3H, 3 × Ar-H), 6.88-6.84 (m, 1H, Ar-H), 4.02 (s, 2H, phCH_2), 3.94 (t, J = 5.2 Hz, 2H, OCH_2), 3.15-3.13 (m, 2H, phCH_2), 3.01-2.99 (m, 2H, NCH_2), 2.94-2.91 (m, 2H, NCH_2), 1.97-1.95 (m, 2H, CH_2), 1.82-1.78 (m, 2H, CH_2). MS (ESI) m/z: 428.2 $[M + H]^+$

*(E)-3-(3-((5-(3,4-dihydroisoquinolin-2(1H)-yl)pentyl)oxy)phenyl)-1-(2-hydroxyphenyl)prop-2-en-1-one (**TM-3**).* Yellow oil, 42.1% yield, 97.6% HPLC purity. ^{1}H NMR (400 MHz, $CDCl_3$) δ 12.81 (s, 1H, OH), 7.96 (d, J = 7.6 Hz, 1H, Ar-H), 7.88 (d, J = 15.6 Hz, 1H, CH=CH), 7.67 (d, J = 15.2 Hz, 1H, CH=CH), 7.54-7.48 (m, 1H, Ar-H), 7.36-7.31 (m, 2H, 2 × Ar-H), 7.29-7.23 (m, 2H, 2 × Ar-H), 7.20-7.16 (m, 2H, 2 × Ar-H), 7.10 (d, J = 7.2 Hz, 1H, Ar-H), 7.03 (d, J = 8.4 Hz, 2H, 2 × Ar-H), 6.96 (t, J = 5.6 Hz, 1H, Ar-H), 4.04 (s, 2H, phCH_2), 3.92 (t, J = 5.2 Hz, 2H, OCH_2), 3.15-3.13 (m,

2H, $phCH_2$), 2.34 (t, J = 7.6 Hz, 2H, NCH_2), 2.13-2.08 (m, 2H, NCH_2), 1.91-1.83 (m, 4H, 2 × CH_2), 1.64-1.59 (m, 2H, CH_2). MS (ESI) m/z: 442.2 $[M + H]^+$

*(E)-3-(3-((6-(3,4-dihydroisoquinolin-2(1H)-yl)hexyl)oxy)phenyl)-1-(2-hydroxyphenyl) prop-2-en-1-one (**TM-4**).* Yellow oil, 45.3% yield, 98.3% HPLC purity. ^{1}H NMR (400 MHz, $CDCl_3$) δ 12.79 (s, 1H, OH), 7.91 (d, *J* = 8.4 Hz, 1H, Ar-H), 7.87 (d, J = 16.0 Hz, 1H, CH=CH), 7.62 (d, J = 15.6 Hz, 1H, CH=CH), 7.49 (t, J = 7.6 Hz, 1H, Ar-H), 7.32 (t, J = 8.0 Hz, 1H, Ar-H), 7.23 (d, J = 7.6 Hz, 1H, Ar-H), 7.17 (s, 1H, Ar-H), 7.11-7.08 (m, 3H, 3 × Ar-H), 7.03-7.01 (m, 2H, 2 × Ar-H), 6.97 (d, J = 9.2 Hz, 1H, Ar-H), 6.92 (d, J = 7.6 Hz, 1H, Ar-H), 4.01 (t, J = 6.0 Hz, 2H, OCH_2), 3.66 (s, 2H, $phCH_2$), 2.91 (t, J = 5.2 Hz, 2H, $phCH_2$), 2.77 (t, J = 5.6 Hz, 2H, NCH_2), 2.55 (t, J = 7.6 Hz, 2H, NCH_2), 1.85-1.80 (m, 2H, CH_2), 1.70-1.62 (m, 2H, CH_2), 1.56-1.51 (m, 2H, CH_2), 1.46-1.39 (m, 2H, CH_2). ^{13}C NMR (100 MHz, $CDCl_3$) 193.7, 163.6, 159.6, 145.5, 136.4, 136.0, 134.4, 134.2, 130.0, 129.7, 128.7, 126.6, 126.2, 125.7, 121.3, 120.4, 120.1, 118.9, 117.1, 114.4, 68.1, 58.1, 55.9, 50.8, 29.2, 28.8, 27.3, 26.9, 26.0. MS (ESI) m/z: 456.2 $[M + H]^+$

*(E)-3-(3-(4-(4-benzylpiperidin-1-yl)butoxy)phenyl)-1-(2-hydroxyphenyl)prop-2-en-1-o ne (**TM-5**).* Yellow oil, 40.8% yield, 97.8% HPLC purity. ^{1}H NMR (400 MHz, $CDCl_3$) δ 12.81 (s, 1H, OH), 8.00-7.91 (m, 1H, Ar-H), 7.87 (d, J = 15.2 Hz, 1H, CH=CH), 7.66 (d, J = 15.2 Hz, 1H, CH=CH), 7.54-7.49 (m, 2H, 2 × Ar-H), 7.35-7.28 (m, 3H, 3 × Ar-H), 7.24-7.19 (m, 2H, 2 × Ar-H), 7.16-7.11 (m, 2H, 2 × Ar-H), 7.07-7.00 (m, 2H, 2 × Ar-H), 6.96 (t, J = 8.4 Hz, 1H, Ar-H), 4.04 (t, J = 6.0 Hz, 2H, OCH_2), 3.51 (d, J = 5.6 Hz, 2H, $phCH_2$), 2.98-2.95 (m, 2H, NCH_2), 2.60 (d, J = 6.8 Hz, 2H, NCH_2), 2.56-2.51 (m, 2H, NCH_2), 2.05-2.01 (m, 4H, 2 × CH_2), 1.86-1.80 (m, 5H, 2 × CH_2 + CH). MS (ESI) m/z: 470.3 $[M + H]^+$

*(E)-1-(4-(3-(3,4-dihydroisoquinolin-2(1H)-yl)propoxy)-2-hydroxyphenyl)-3-(4-fluoro phenyl)prop-2-en-1-one (**TM-6**).* Yellow oil, 52.1% yield, 97.5% HPLC purity. ^{1}H NMR (400 MHz, $CDCl_3$) δ ^{1}H NMR 12.34 (s, 1H, OH), 7.85 (d, J = 15.2 Hz, 1H, Ar-H), 7.82 (d, J = 8.0 Hz, 1H, Ar-H), 7.66 (d, J = 5.6 Hz, 1H, Ar-H), 7.64 (d, J = 5.6 Hz, 1H, Ar-H), 7.49 (d, J = 15.2 Hz, 1H, CH=CH), 7.29-7.26 (m, 2H, 2 × Ar-H), 7.19

(d, J = 6.8 Hz, 1H, Ar-H), 7.15-7.09 (m, 3H, 3 × Ar-H), 6.46 (d, J = 8.8 Hz, 1H, Ar-H), 6.43 (d, J = 1.6 Hz, 1H, Ar-H), 4.23 (s, 2H, $phCH_2$), 4.16 (t, J = 5.6 Hz, 2H, OCH_2), 3.37-3.35 (m, 2H, $phCH_2$), 3.22-3.20 (m, 4H, 2 × NCH_2), 2.46 (m, 2H, CH_2). MS (ESI) m/z: 432.2 $[M + H]^+$

*(E)-1-(4-(4-(3,4-dihydroisoquinolin-2(1H)-yl)butoxy)-2-hydroxyphenyl)-3-(2-methoxyphenyl)prop-2-en-1-one (**TM-7**).* Yellow oil, 56.4% yield, 98.6% HPLC purity. ^1H NMR (400 MHz, $CDCl_3$) δ 13.58 (s, 1H, OH), 8.18 (d, J = 15.6 Hz, 1H, CH=CH), 7.79 (d, J = 8.8 Hz, 1H, Ar-H), 7.67 (d, J = 15.6 Hz, 1H, CH=CH), 7.61 (d, J = 7.6 Hz, 1H, Ar-H), 7.36 (t, J = 7.6 Hz, 1H, Ar-H), 7.12-7.09 (m, 3H, 3 × Ar-H), 7.02-6.95 (m, 2H, 2 × Ar-H), 6.92 (d, J = 8.4 Hz, 1H, Ar-H), 6.47-6.43 (m, 2H, 2 × Ar-H), 4.02 (t, J = 5.6 Hz, 2H, OCH_2), 3.89 (s, 3H, OCH_3), 3.67 (s, 2H, $phCH_2$), 2.91 (t, J = 5.6 Hz, 2H, $phCH_2$), 2.77 (t, J = 5.6 Hz, 2H, NCH_2), 2.60 (t, J = 6.8 Hz, 2H, NCH_2), 1.87-1.78 (m, 4H, 2 × CH_2). ^{13}C NMR (100 MHz, $CDCl_3$) 192.4, 166.6, 165.6, 158.9, 140.0, 134.3, 134.1, 132.0, 131.4, 129.4, 128.7, 126.6, 126.3, 125.7, 123.8, 120.9, 120.8, 114.2, 111.3, 107.9, 101.6, 68.1, 57.6, 55.9, 55.6, 50.8, 29.8, 28.8, 27.0, 23.5. MS (ESI) m/z: 458.2 $[M + H]^+$

*(E)-1-(4-((6-(3,4-dihydroisoquinolin-2(1H)-yl)hexyl)oxy)-2-hydroxyphenyl)-3-(4-(dimethylamino)phenyl)prop-2-en-1-one (**TM-8**).* Yellow oil, 32.7% yield, 98.2% HPLC purity. ^1H NMR (400 MHz, $CDCl_3$) δ 13.77 (s, 1H, OH), 7.86 (d, J = 15.2 Hz, 1H, CH=CH), 7.81 (d, J = 8.8 Hz, 1H, Ar-H), 7.55 (d, J = 8.4 Hz, 2H, 2 × Ar-H), 7.36 (d, J = 15.6 Hz, 1H, CH=CH), 7.12-7.10 (m, 3H, 3 × Ar-H), 7.02 (d, J = 5.2 Hz, 1H, Ar-H), 6.68 (d, J = 8.4 Hz, 2H, 2 × Ar-H), 6.45 (d, J = 9.6 Hz, 2H, 2 × Ar-H), 4.00 (t, J = 6.4 Hz, 2H, OCH_2), 3.68 (s, 2H, NCH_2ph), 3.04 (s, 6H, 2 × NCH_3), 2.93 (t, J = 5.2 Hz, 2H, $phCH_2$), 2.79 (t, J = 5.2 Hz, 2H, NCH_2), 2.56 (t, J = 7.6 Hz, 2H, NCH_2), 1.83-1.79 (m, 2H, CH_2), 1.70-1.64 (m, 2H, CH_2), 1.55-1.47 (m, 2H, CH_2), 1.46-1.42 (m, 2H, CH_2). ^{13}C NMR (100 MHz, $CDCl_3$) 191.8, 166.5, 165.3, 152.2, 145.3, 134.1, 134.0, 130.9, 130.6 (2C), 128.7, 126.6, 126.3, 125.7, 122.6, 114.7, 114.3, 111.9 (2C), 107.7, 101.6, 68.2, 58.0, 55.8, 50.7, 40.1 (2C), 29.0, 28.6, 27.2, 26.8, 25.9. MS (ESI) m/z: 499.3 $[M + H]^+$

3-(3-(4-(3,4-Dihydroisoquinolin-2(1H)-yl)butoxy)phenyl)-1-(2-hydroxyphenyl)propan -1-one (**TM-9**). To a mixture of **TM-2** (1.5 mmol) in EtOH, Pd/C (0.075 mmol) was added to the mixture in the presence of H_2. The reaction was stirred for 28h at room temperature, the mixture was treated and the organic phase was evaporated under reduced pressure. The residue was purified using mixtures of petroleum ether/acetone (50:1) as eluent on a silica gel chromatography to obtain **TM-9**. Light yellow oil, 40.1% yield, 98.2% HPLC purity. ^{1}H NMR (400 MHz, $CDCl_3$) δ ^{1}H NMR (400 MHz, $CDCl_3$) δ 12.79 (s, 1H, OH), 7.52 (d, J = 7.6 Hz, 1H, Ar-H), 7.20-7.15 (m, 4H, 4 × Ar-H), 7.13-7.11 (m, 1H, Ar-H), 7.04 (d, J = 7.6 Hz, 2H, 2 × Ar-H), 7.00 (d, J = 4.4 Hz, 1H, Ar-H), 6.95 (d, J = 8.0 Hz, 1H, Ar-H), 6.91 (s, 1H, Ar-H), 6.87-6.83 (m, 1H, Ar-H), 4.03 (t, J = 6.0 Hz, 2H, OCH_2), 3.99 (t, J = 6.0 Hz, 2H, $phCH_2$), 3.89-3.86 (m, 4H, 2 × $phCH_2$), 3.02-3.00 (m, 4H, 2 × NCH_2), 2.80-2.77 (m, 2H, $COCH_2$), 1.93-1.85 (m, 4H, 2 × CH_2). MS (ESI) m/z: 430.2 $[M + H]^+$

4.2 Biological activity

4.2.1 Inhibition assay of AChE and BuChE. The inhibitory potency of synthetic compounds against AChE and BuChE was assessed by modified Ellman assay [22, 39]. For AChE inhibition assays, a reaction mixture (100 µL) containing ATC (1 mmol/L, 30 µL), pH = 8.0 phosphate-buffered solution, 10 µL *Ee*AChE (0.45 U/mL) and different concentrations of test compounds (20 µL) was incubated at 37°C for 15 min. Then 5,5'-dithiobis-2-nitrobenzoic acid (DTNB, 0.2%, 30 µL) was added. The inhibitory activities were determined by using a Varioskan Flash Multimode Reader at 412 nm. The inhibition percentage was calculated by the following formula: $(1-A_i/A_c) \times 100$, where A_i and A_c are the absorbance obtained for AChE in the presence and absence of inhibitors, respectively. *In vitro* BuChE assay was performed using a method similar as described above.

4.2.2 Recombinant human MAO-A and MAO-B inhibition studies. Recombinant human MAO-A and MAO-B were purchased from Sigma-Aldrich and stored at -80 °C [26]. Solutions of test compounds were prepared in DMSO (2.5 mM) and diluted with potassium phosphate buffer (100 mM, pH 7.40, containing KCl 20.2 mM) to a final volume of 500 µL containing various concentrations of test compounds

(0-100 μM) and kynuramine (45 μM for MAO-A and 30 μM for MAO-B). The reactions were initiated by the addition of the enzyme (7.5 μg/mL) and then incubated for 30 min at 37. Then 400 μL NaOH (2N) and 1000 μL water were added to terminate the enzymatic reactions and the mixtures were centrifuged at 16000g for 10 min.[5] The concentrations of the MAOs generated 4-hydroxyquinoline were determined by measuring the fluorescence of the supernatant on a Varioskan Flash Multimode Reader (PerkinElmer) with excitation and emission wavelengths at 310 nm and 400 nm, respectively. A linear calibration curve was constructed by preparing samples containing 4-hydroxyquinoline (0.047–1.56 μM) dissolved in 500 μL potassium phosphate buffer. To each calibration standard, 400 μL NaOH (2 N) and 1000 μL water were added. The appropriate control samples were included to confirm that the test compounds do not fluoresce or quench the fluorescence of 4-hydroxyquinoline under the assay conditions. IC_{50} values were calculated from sigmoidal dose-response curves (graphs of the initial rate of kynuramine oxidation versus the logarithm of inhibitor concentration). Each sigmoidal curve was constructed form six different compound concentrations spanning at least three orders of magnitude. Data analyses were performed with GraphRad Prism 5 employing the one site competition model. IC_{50} values were determined in triplicate and expressed as mean ± SD.

4.2.3. Antioxidant activity assay

The antioxidant activity was tested by the oxygen radical absorbance capacity fluorescein (ORAC-FL) assay. The details referenced our previous work [24].

4.2.4. Metal binding study

The metal binding studies were performed in a Varioskan Flash Multimode Reader (Thermo Scientific). The $CuCl_2$, $ZnCl_2$, $AlCl_3$, $FeSO_4$, CuCl, and $Fe(NO_3)_3$ were used to test the metal binding assay. In addition, the stoichiometry of the compound-Cu^{2+} complex could reference our previous work [24, 34].

4.2.5. Effect of test compounds on self-induced A$\beta_{1\text{-}42}$ aggregation assay. Thioflavin T-based flurometric assay was performed to investigate the self-induced A$\beta_{1\text{-}42}$ aggregation [24, 29]. Briefly, the A$\beta_{1\text{-}42}$ treated (20 μL, 25 μM, final concentration) was incubated at 37 °C for 24 h with or without 20 μL of test compounds at different concentrations ranging from 1-50 μM in 50 mM pH = 7.4. After incubated, 160 μL of 5 μM thioflavin T in 50 mM glycine-NaOH buffer (pH 8.5) was added. Fluorescence was measured by a Varioskan Flash Multimode Reader (Thermo Scientific) with excitation and emission wavelengths at 446 and 490 nm, respectively. Each assay was run in triplicate. The presence of the inhibitor was calculated by the following expression $(1\text{-}IF_i/IF_c) \times 100$, in which IF_i and IF_c are the fluorescence intensities obtained for A$\beta_{1\text{-}42}$ in the presence and absence of inhibitors after subtracting the background, respectively.

4.2.6. Effect of test compounds on Cu^{2+}-induced A$\beta_{1\text{-}42}$ aggregation. The mixture of A$\beta_{1\text{-}42}$ (20 μL, 25 μM) and Cu^{2+} (20 μL, 25 μM) was incubated at 37 °C for 24h with or without the tested compound. After incubated, 190 μL of 5 μM Thioflavin T in 50 mM glycine-NaOH buffer (pH 8.5) was added. The detection method was performed according to the self-induced A$\beta_{1\text{-}42}$ experiment [24, 32].

As for the disaggregation of Cu^{2+}-induced Aβ fibrils experiment, the mixture of the A$\beta_{1\text{-}42}$ (20 μL, 25 μM) with Cu^{2+} (20 μL, 25 μM) was incubated 37 °C for 24 h. The tested compound (20 μL, 25 μM) was then added and incubated at 37 °C for another 24 h. After incubation, 190 μL of 5 μM thioflavin T in 50 mM glycine-NaOH buffer (pH 8.5) was added. The detection method was the same as above.

4.2.7. Transmission Electron Microscopy (TEM) Assay. The preparation of samples could reference the self-induced and Cu^{2+}-induced A$\beta_{1\text{-}42}$ aggregation experiments. Aliquots (10 μL) of the samples were placed on a carbon-coated copper/rhodium grid for 2 min at room temperature. Excess sample was removed using filter paper followed by washing twice with ddH_2O. Each grid was incubated with uranyl acetate (1% w/v ddH_2O). Upon removal of excess uranyl acetate, the grids were dried for 15 min at room temperature. Images from each sample were taken on a Field Emission

Transmission Electron Microscope (JEM-2100F).

4.2.8. H_2O_2 induced PC12 cell injury. MTT reduction assay was used to evaluate the protection effect of **TM-2** [34]. The cells were grown at 37 °C in a humidified atmosphere of 5% CO_2. Neuronal PC12 cells were plated at a density of 10^5 cells/well on 96-well plates in 100 μL of DEME. The cells were pre-incubated with **TM-2** for 24 h before H_2O_2 (100 μM) was added. The cells were treated with or without H_2O_2 for two hours, and then replaced with fresh DMEM medium. Assays for cell viability were performed 24 h after cultured at 37 °C in fresh medium. The cells were treated with 25 μL MTT (5 mg/mL in PBS) for 4 h at 37 °C and then were lysed in a buffered solution containing *N*, *N*-dimethylformamide (pH 4.5, 50% (aq, v/v)) and sodium dodecyl sulfate (SDS, 20% (w/v)) overnight at room temperature in the dark. The absorbance (A590 nm) was measured using Elx800 microplate reader (Bio-Tek). % inhibition = $[1-(A_{sample}/A_{control})]\times100$.

4.2.9. In vitro blood−brain barrier permeation assay

The blood-brain barrier penetration of compounds was evaluated using the paral lel artificial membrane permeation assay (PAMPA) described by Di *et al* [36]. The detailed procedure refers to our previous work.

4.2.10. Step-down passive avoidance test. Kunming mice at body weight of 18–22 g (six weeks old, either gender) were supplied by the Center of Experimental Animals of Sichuan Academy of Chinese Medicine Sciences (eligibility certification no. SCXK[chuan] 2015-030). Mice were maintained under standard conditions with a 12 h: 12 h light–dark cycle at 20−22 °C with a relative humidity of 60−70%. Sterile food and water were provided according to institutional guidelines.

A step-down passive avoidance test was performed to test the ability of memory in mice [39]. The apparatus consisted of a grid floor with a wooden block placed in the center. The block served as a shock free zone. The mice underwent two separate trials: a training trial and a test trial 24 h later. For training trial, mice were initially placed on the block and were given an electrical foot shock (0.5 mA, 2s) through the grid

floor on stepping down. We used a total of 60 mice in the passive avoidance test with 10 mice were used per treatment. Compounds **TM-2** (1.9, 5.6 and 161.8 mg/kg, *p.o.*) or donepezil (5.0 mg/kg, *p.o.*) as a positive control were orally given 1 h before each training trial. After 30 min, memory impairment was induced by administering scopolamine (3 mg/kg, *i.p.*). Twenty-four hours after the training trial, mice were placed on the block and the time for the animal to step down was measured as latency time for test trial. An upper cut-off time was set at 300 s.

All data are expressed as mean ± SEM. Differences between groups were examined for statistical significance using one-way ANOVA with Student's *t* test. A *P* value less than 0.05 denoted the presence of a statistically significant difference.

AUTHOR INFORMATION

Corresponding Author

***** For Zhipei Sang: E-mail: sangzhipei@126.com

***** For Wenmin Liu: E-mail: liuwm1969@163.com

***** For Zhenghuai Tan: E-mail: tanzhh616@163.com

Author Contributions

The manuscript was written through contributions of all authors. All authors have given approval to the final version of the manuscript. #These authors contributed equally.

Notes

The authors declare no competing financial interest.

ACKNOWLEDGMENTS

This work was supported in part by the Foundation and Frontier Projects of Nanyang Science and Technology Bureau (2017JCQY020 and 2017 JCQY021), the Special Project of Nanyang Normal University (SYKF2018081 and STP2018004).

Supporting Information Available:

The representative ^{1}H, ^{13}C NMR and HPLC spectra for the synthesized compounds are available as supplementary material.

References

[1] Alzheimer's Association. 2015 Alzheimer's disease facts and figures. Alzheimer's Dementia **2015**, *11*, 332-384.

[2] Lane CA, Hardy J, Schott JM. Alzheimer's disease. Eur J Neurol. 2018, 25(1): 59-70.

[3] Graham WV, Bonito-Oliva A, Sakmar TP. Update on Alzheimer's disease therapy and prevention strategies. Annu Rev Med. 2017, 68: 413-430.

[4] Ballard C, Gauthier S, Corbett A, Brayne C, Aarsland D, Jones E. Alzheimer's disease. Lancet 2011, 377(9770): 1019-1031.

[5] Ferreira-Vieira TH, Guimaraes IM, Silva FR, Ribeiro FM. Alzheimer's disease: targeting the cholinergic system. Curr Neuropharmacol. 2016, 14(1): 101-115.

[6] Hampel H, Mesulam MM, Cuello AC, Farlow MR, Giacobini E, Grossberg GT, Khachaturian AS, Vergallo A, Cavedo E, Snyder PJ, Khachaturian ZS. The cholinergic system in the pathophysiology and treatment of Alzheimer's disease. Brain. 2018, 141(7): 1917-1933.

[7] Dighe, S.N.; Deora, G.S.; De la Mora, E.; Nachon, F.; Can, S.; Parat, M.O.; Brazzolotto, X.; Ross, B.P. Discovery and structure-activity relationships of a highly selective butyrycholinesterase inhibitor by structure-based virtual screening. J. Med. Chem. 2016, 59: 7683-7689.

[8] Chen, V. P.; Gao, Y.; Geng, L.; Parks, R. J.; Pang, Y.-P.; Brimijoin, S. Plasma butyrylcholinesterase regulates ghrelin to control aggression. Proc. Natl. Acad. Sci. U. S. A. 2015, 112(7): 2251−2256.

[9] 'Paroni G, Bisceglia P, Seripa D. Understanding the amyloid hypothesis in Alzheimer's disease. J Alzheimers Dis. 2019, 68(2): 493-510.

[10] Ricciarelli R, Fedele E. The amyloid cascade hypothesis in Alzheimer's disease: it's time to change our mind. Curr Neuropharmacol. 2017, 15(6): 926-935.

[11] Cheignon C, Tomas M, Bonnefont-Rousselot D, Faller P, Hureau C, Collin F. Oxidative stress and the amyloid beta peptide in Alzheimer's disease. Redox Biol. 2018, 14: 450-464.

[12] Spinello A, Bonsignore R, Barone G, Keppler BK, Terenzi A. Metal ions and metal complexes in Alzheimer's disease. Curr Pharm Des. 2016, 22(26): 3996-4010.

[13] Sensi SL, Granzotto A, Siotto M, Squitti R. Copper and Zinc dysregulation in Alzheimer's disease. Trends Pharmacol Sci. 2018, 39(12): 1049-1046.

[14] Kumar B, Gupta VP, Kumar V. A perspective on monoamine oxidase enzyme as drug target: challenges and opportunities. Curr Drug Targets. 2017, 18(1): 87-97.

[15] Pazini AM, Gomes GM, Villarinho JG, da Cunha C, Pinheiro F, Ferreira AP, Mello CF, Ferreira J, Rubin MA. Selegiline reverses a$\beta_{25\text{-}35}$-induced cognitive deficit in male mice. Neurochem Res. 2013, 38(11): 2287-2294.

[16] de Freitas Silva, M.; Dias, K.S.T.; Gontijo, V.S.; Ortiz, C.J.C.; Viega, C. Multi-target directed drugs as a modern approach for drug design towards Alzheimer's disease: an update. *Curr Med Chem.* **2018**, 25(29): 3491-3525.

[17] Umar, T.; Hoda, N. Alzheimer's disease: A systemic review of substantial therapeutic targets and the leading multi-functional molecules. Curr Top Med Chem. 2017, 17(31): 3370-3389.

[18] Agis-Torres A, Sölhuber M, Fernandez M, Sanchez-Montero JM. Multi-target-directed ligands and other therapeutic strategies in the search of a real

solution for Alzheimer's disease. Curr Neuropharmacol. 2014, 12(1): 2-36.

[19] Zhuang C, Zhang W, Sheng C, Zhang W, Xing C, Miao Z. Chalcone: a privileged structure in medicinal chemistry. Chem Rev 2017, 117(12): 7762-7810.

[20] Zhang X, Rakesh KP, Bukhari SNA, Balakrishna M, Manukumar HM, Qin HL. Multi-targetable chalcone analogs to treat deadly Alzheimer's disease: Current view and upcoming advice. Bioorg Chem. 2018, 80: 86-93.

[21] Sang, Z.; Pan, W.; Wang, K.; Ma, Q.; Yu, L.; Yang, Y.; Bai, P.; Leng, C.; Xu, Q.; Li, X.; Tan, Z.; Liu, W. Design, synthesis and evaluation of novel ferulic acid-O-alkylamine derivatives as potential multifunctional agents for the treatment of Alzheimer's disease. Eur. J. Med. Chem. 2017, 130, 379-392.

[22] Cavdar H, Senturk M, Guney M, Durdagi S, Kayik G, Supuran CT, Ekinci D. Inhibition of acetylcholinesterase and butyrylcholinesterase with uracil derivatives: kinetic and computational studies. J Enzyme Inhib Med Chem. 2019, 34(1): 429-437.

[23] Chen SC, Qiu GL, Li B, Shi JB, Liu XH, Tang WJ. Tricyclic pyrazolo[1,5-d][1,4]benzoxazepin-5(6H)-one scaffold derivatives: Synthesis and biological evaluation as selective BuChE inhibitors. Eur J Med Chem. 2018, 147: 194-204.

[24] Sang Z, Qiang X, Li Y, Yuan W, Liu Q, Shi Y, Ang W, Luo Y, Tan Z, Deng Y. Design, synthesis and evaluation of scutellarein-O-alkylamines as multifunctional agents for the treatment of Alzheimer's disease. Eur J Med Chem. 2015, 94: 348-366.

[25] Martini, F.; Bruning, C.A.; Soares, S.M.; Nogueira, C.W.; Zeni, G. Inhibitory effect of ebselen on cerebral acetylcholinesterase activity in vitro: kinetics and reversibility of inhibition. Curr. Pharm. Des. 2015, 21(7): 920-924.

[26] Li Y, Qiang X, Luo L, Yang X, Xiao G, Zheng Y, Cao Z, Sang Z, Su F, Deng Y. Multitarget drug design strategy against Alzheimer's disease: Homoisoflavonoid

Mannich base derivatives serve as acetylcholinesterase and monoamine oxidase B dual inhibitors with multifunctional properties. Bioorg Med Chem. 2017, 25(2): 714-726.

[27] Hu J, Pan T, An B, Li Z, Li X, Huang L. Synthesis and evaluation of clioquinol-rolipram/roflumilast hybrids as multitarget-directed ligands for the treatment of Alzheimer's disease. Eur J Med Chem. 2019, 163: 512-526.

[28] Liu H, Qiang X, Song Q, Li W, He Y, Ye C, Tan Z, Deng Y. Discovery of 4'-OH-flurbiprofen Mannich base derivatives as potential Alzheimer's disease treatment with multiple inhibitory activities. Bioorg Med Chem 2019, 27(6): 991-1001.

[29] Xu P, Zhang M, Sheng R, Ma Y. Synthesis and biological evaluation of deferiprone-resveratrol hybrids as antioxidants, Aβ1-42 aggregation inhibitors and metal-chelating agents for Alzheimer's disease. Eur J Med Chem. 2017, 127: 174-186.

[30] Li T., Pan W., Wang K., Liu W., Ma Q., Sang Z. Novel ferulic acid-donepezil hybrids as multifunctional agents for the treatment of Alzheimer's disease with butyrylcholinesterase, amyloid-β, antioxidant and neuroprotective properties. Lett Drug Des Discov. 2017, 14 (8): 918-929.

[31] Iraji A, Firuzi O, Khoshneviszadeh M, Tavakkoli M, Mahdavi M, Nadri H, Edraki N, Miri R. Multifunctional iminochromene-2H-carboxamide derivatives containing different aminomethylene triazole with BACE1 inhibitory, neuroprotective and metal chelating properties targeting Alzheimer's disease. Eur J Med Chem. 2017, 141: 690-702.

[32] Wang Z, Wang Y, Li W, Mao F, Sun Y, Huang L, Li X. Design, synthesis, and evaluation of multitarget-directed selenium-containing clioquinol derivatives for the treatment of Alzheimer's disease. ACS Chem Neurosci. 2014, 5(10): 952-962.

[33] Huang L, Lu C, Sun Y, Mao F, Luo Z, Su T, Jiang H, Shan W, Li X.

Multitarget-directed benzylideneindanone derivatives: anti-β-amyloid (Aβ) aggregation, antioxidant, metal chelation, and monoamine oxidase B (MAO-B) inhibition properties against Alzheimer's disease. J Med Chem. 2012, 55(19): 8483-8492.

[34] Sang Z, Qiang X, Li Y, Xu R, Cao Z, Song Q, Wang T, Zhang X, Liu H, Tan Z, Deng Y. Design, synthesis and evaluation of scutellarein-O-acetamidoalkylbenzylamines as potential multifunctional agents for the treatment of Alzheimer's disease. Eur J Med Chem. 2017, 135: 307-323.

[35] Hepnarova V, Korabecny J, Matouskova L, Jost P, Muckova L, Hrabinova M, Vykoukalova N, Kerhartova M, Kucera T, Dolezal R, Nepovimova E, Spilovska K, Mezeiova E, Pham NL, Jun D, Staud F, Kaping D, Kuca K, Soukup O. The concept of hybrid molecules of tacrine and benzyl quinolone carboxylic acid (BQCA) as multifunctional agents for Alzheimer's disease. Eur J Med Chem. 2018, 150: 292-306.

[36] Di L, Kerns EH, Fan K, McConnell OJ, Carter GT. High throughput artificial membrane permeability assay for blood-brain barrier. Eur J Med Chem. 2003, 38(3): 223-232.

[37] Matos MJ, Vilar S, Gonzalez-Franco RM, Uriarte E, Santana L, Friedman C, Tatonetti NP, Viña D, Fontenla JA. Novel (coumarin-3-yl)carbamates as selective MAO-B inhibitors: synthesis, in vitro and in vivo assays, theoretical evaluation of ADME properties and docking study. Eur J Med Chem. 2013, 63: 151-161.

[38] Ishola IO, Osele MO, Chijioke MC, Adeyemi OO. Isorhamnetin Enhanced Cortico-Hippocampal Learning and Memory Capability in Mice with Scopolamine-Induced Amnesia: Role of Antioxidant Defense, Cholinergic and BDNF Signaling. Brain Res. 2019, doi: 10.1007/s12640-019-0008-6

[39] Sang Z, Wang K, Han X, Cao M, Tan Z, Liu W. Design, Synthesis, and Evaluation of Novel Ferulic Acid Derivatives as Multi-Target-Directed Ligands

for the Treatment of Alzheimer's Disease. ACS Chem Neurosci. 2019, 10(2): 1008-1024.

A **B**

Figures, Schemes and Tables

Figure 1. The design strategy of chalcone derivatives.

Figure 2. (A) Representation of compound **TM-2** (green stick) interacting with residues in the binding site of *Tc*AChE (PDB code: 1EVE). (B) 3D docking model of compound **TM-2** with *Tc*AChE.

Figure 3. (A) Representation of compound **TM-2** (green stick) interacting with residues in the binding site of *hu*BuChE (PDB code: 4tpk). (B) 3D docking model of compound **TM-2** with *hu*BuChE.

Figure 4 (A) *eqBuChE* recovery after compound **TM-2** diluted to 1× or 0.1 × IC_{50}, compared to standard rivastigmine and donepezil. (B) *eqBuChE* recovey of donepezil, rivastigmine, and **TM-2** diluted to 0.1 × IC_{50}, monitoring with time. Data points were expressed as the mean ± SEM of three independent experiments.

Figure 5 Compound **TM-2** (green stick) interacting with residues in the binding site of MAO-B (PDB code: 2V60), highlighting the protein residues that participate in the main interactions with the inhibitor.

Figure 6 Docking studies of compound **TM-2** with A$\beta_{1\text{-}42}$ (PDB ID: 1BA4). (A) **TM-2** (green stick) interacting with residues in the binding site of A$\beta_{1\text{-}42}$ (PDB code: 1BA4). (B) 3D docking model of compound **TM-2** with A$\beta_{1\text{-}42}$.

Figure 7 The UV spectra of compound **TM-2** (37.5 μM, in methanol) alone or in the presence of $CuCl_2$, $AlCl_3$, $ZnCl_2$, $FeSO_4$, CuCl and $Fe(NO_3)_3$ (37.5 μM, in methanol)

Figure 8 Determination of the stoichiometry of complex-Cu^{2+} by using molar ratio method through titrating the methanol solution of compound **TM-2** with ascending amounts of $CuCl_2$. The final concentration of tested compound was 37.5 μM.

Figure 9 (A) Scheme of the inhibition experiment; (B) TEM images of Aβ species from inhibition experiments. (C) Scheme of the disaggregation experiments; (D) TEM images of samples from disaggregation experiments.

Figure 10 (A) Effects of **TM-2** on cell viability in PC12 cells. (B) Protective effects of **TM-2** on cell injury induced by H_2O_2 (100 μM) in PC12 cells. $^{\#\#}p < 0.01$ *vs* control; $^{*}p < 0.05$ *vs* H_2O_2 group and $^{**}p < 0.01$ *vs* H_2O_2 group.

Figure 11 Lineal correlation between experimental and reported permeability of commercial drugs using the PAMPA-BBB assay. $P_e(\text{exp}) = 0.9163P_e(\text{bibl.}) - 0.2247$ ($R^2 = 0.9558$).

Figure 12 Effects of compound **TM-2** on scopolamine-induced memory deficit in the step-down passive avoidance test. Values are expressed as the mean ± SEM (n=10). # $p < 0.05$ *vs* normal group. * $p < 0.05$ and ** $p < 0.01$ *vs* scopolamine-treated control group.

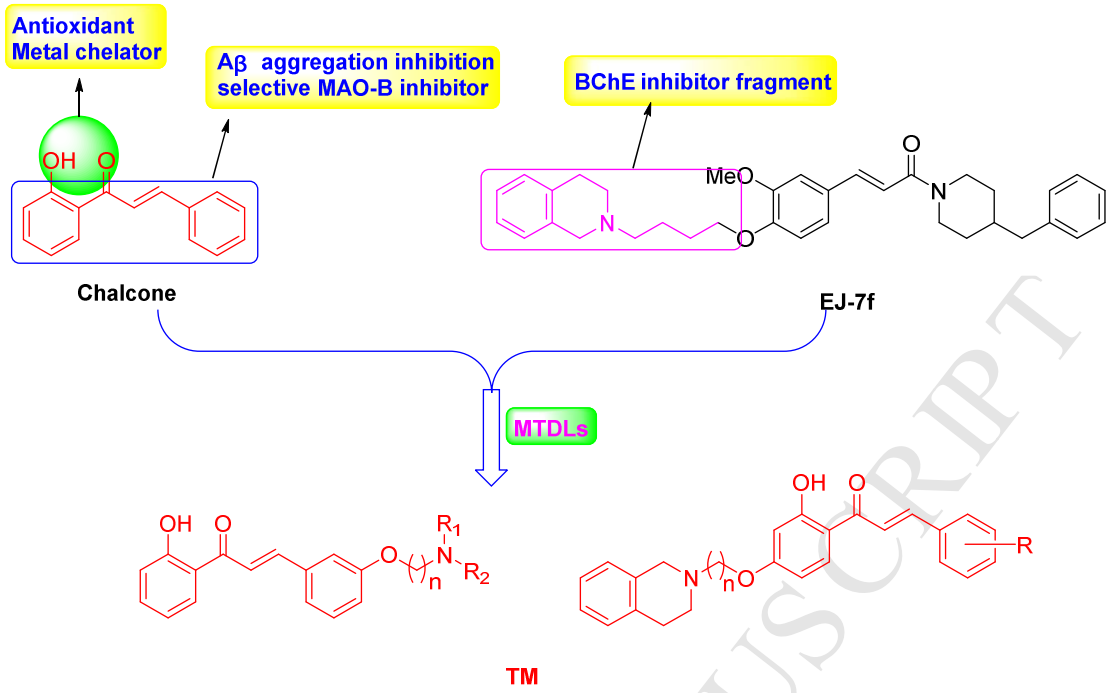

Figure 1. The design strategy of chalcone derivatives.

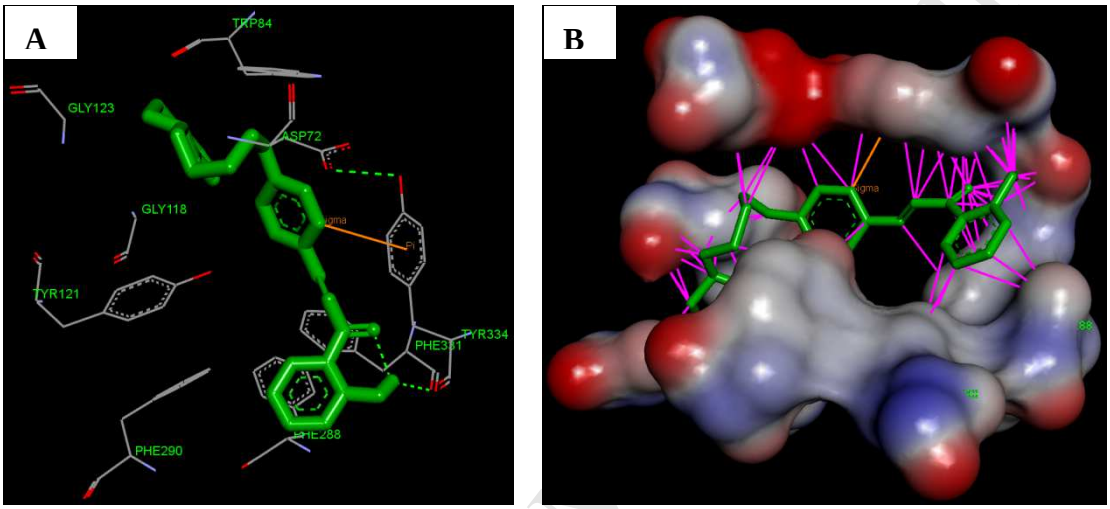

Figure 2. (A) Representation of compound **TM-2** (green stick) interacting with residues in the binding site of *Tc*AChE (PDB code: 1EVE). (B) 3D docking model of compound **TM-2** with *Tc*AChE.

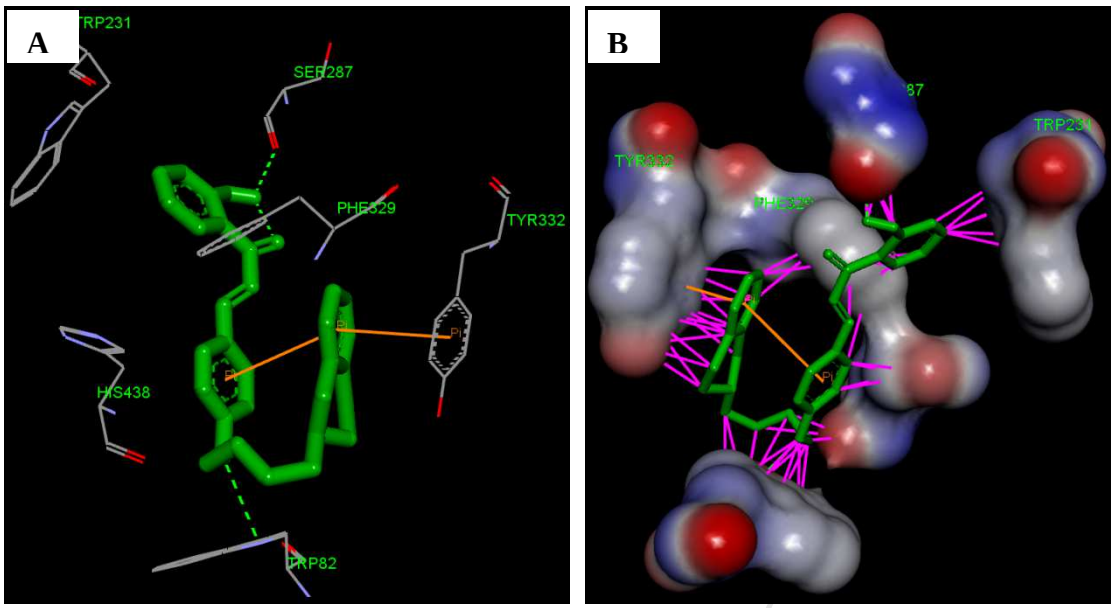

Figure 3. (A) Representation of compound **TM-2** (green stick) interacting with residues in the binding site of *hu*BuChE (PDB code: 4tpk). (B) 3D docking model of compound **TM-2** with *hu*BuChE.

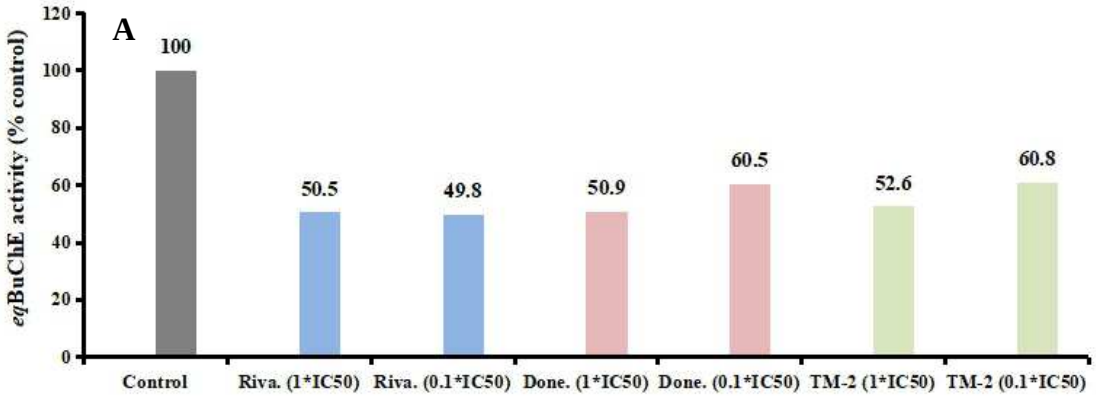

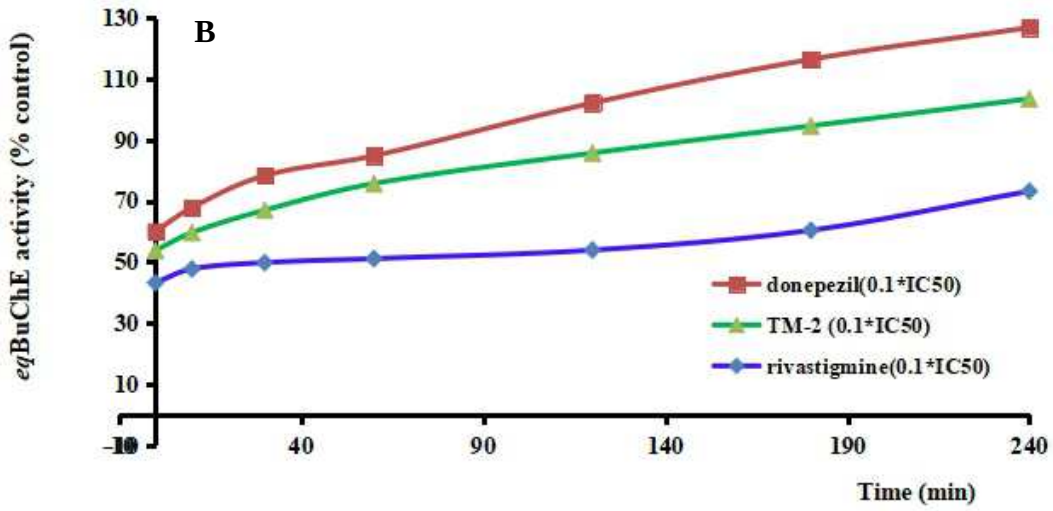

Figure 4 (A) *eqBuChE* recovery after compound **TM-2** diluted to 1× or 0.1 × IC_{50}, compared to standard rivastigmine and donepezil. (B) *eqBuChE* recovey of donepezil, rivastigmine, and **TM-2** diluted to 0.1 × IC_{50}, monitoring with time. Data points were expressed as the mean ± SEM of three independent experiments.

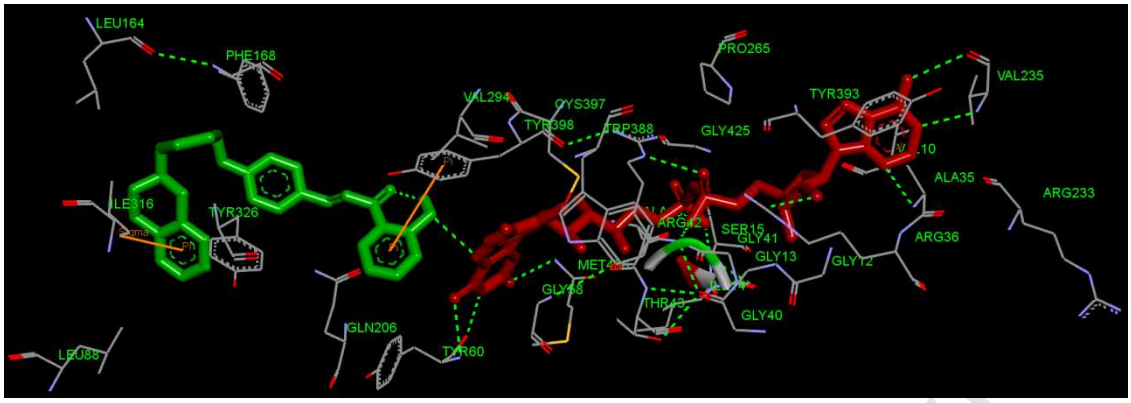

Figure 5 Compound **TM-2** (green stick) interacting with residues in the binding site of MAO-B (PDB code: 2V60), highlighting the protein residues that participate in the main interactions with the inhibitor.

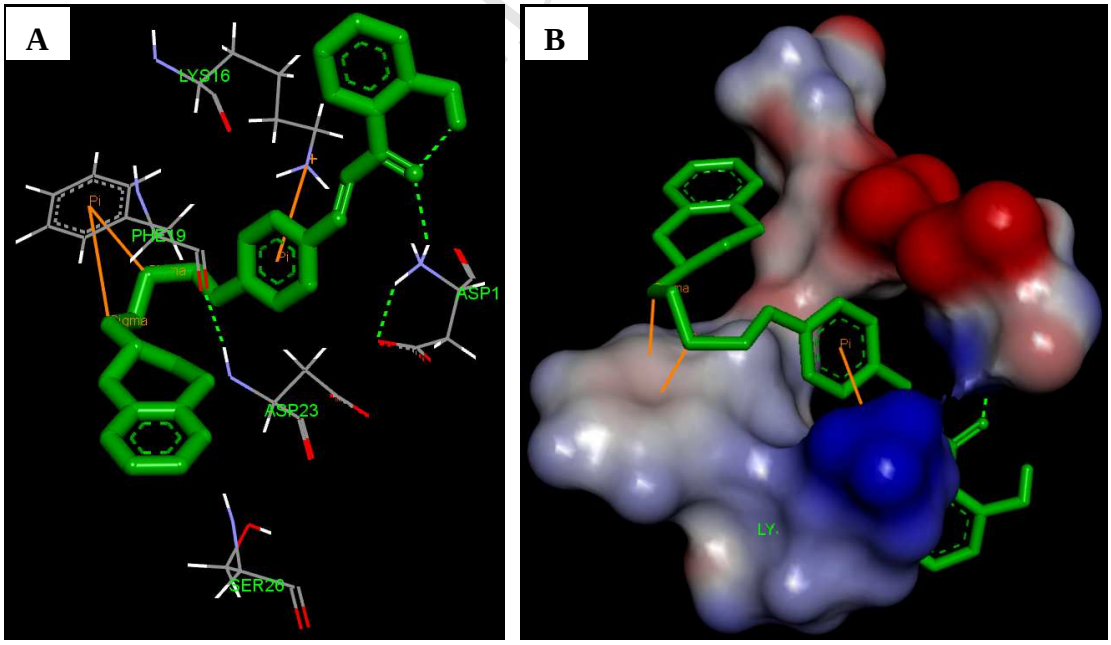

Figure 6 Docking studies of compound **TM-2** with A$\beta_{1\text{-}42}$ (PDB ID: 1BA4). (A) **TM-2** (green stick) interacting with residues in the binding site of A$\beta_{1\text{-}42}$ (PDB code: 1BA4). (B) 3D docking model of compound **TM-2** with A$\beta_{1\text{-}42}$.

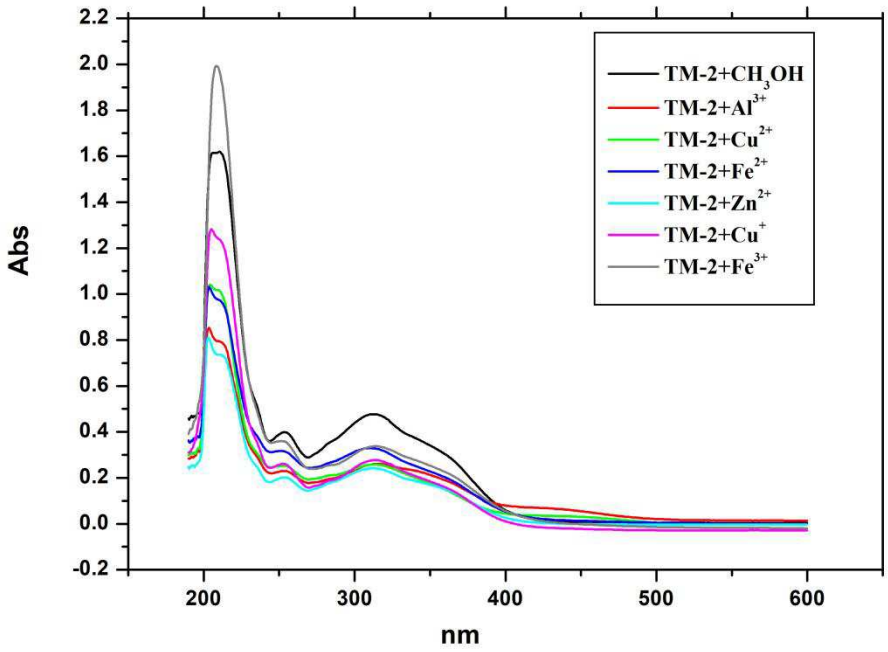

Figure 7 The UV spectrum of compounds **TM-2** (37.5 μM, in methanol) alone or in the presence of Cu^{2+}, Al^{3+}, Fe^{2+}, Zn^{2+}, Cu^{2+}, and Fe^{3+} (37.5 μM, in methanol)

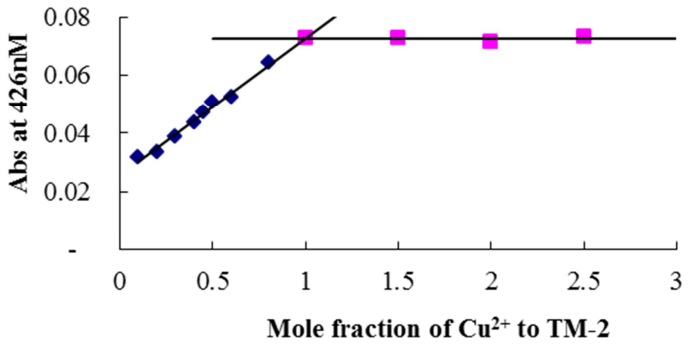

Figure 8 Determination of the stoichiometry of complex-Cu^{2+} by using molar ratio method through titrating the methanol solution of compound **TM-2** with ascending amounts of $CuCl_2$. The final concentration of tested compound was 37.5 μM.

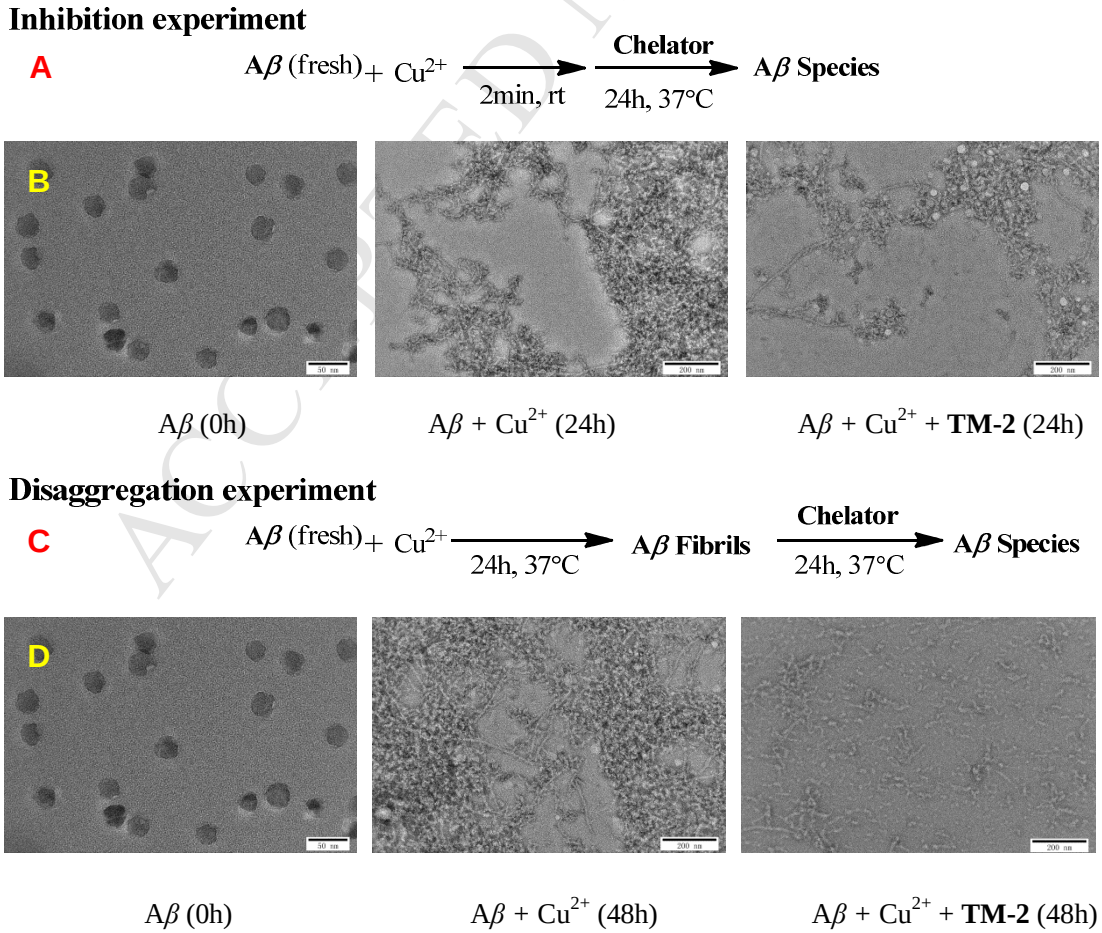

Figure 9 (A) Scheme of the inhibition experiment; (B) TEM images of Aβ species from inhibition experiments. (C) Scheme of the disaggregation experiments; (D) TEM images of samples from disaggregation experiments.

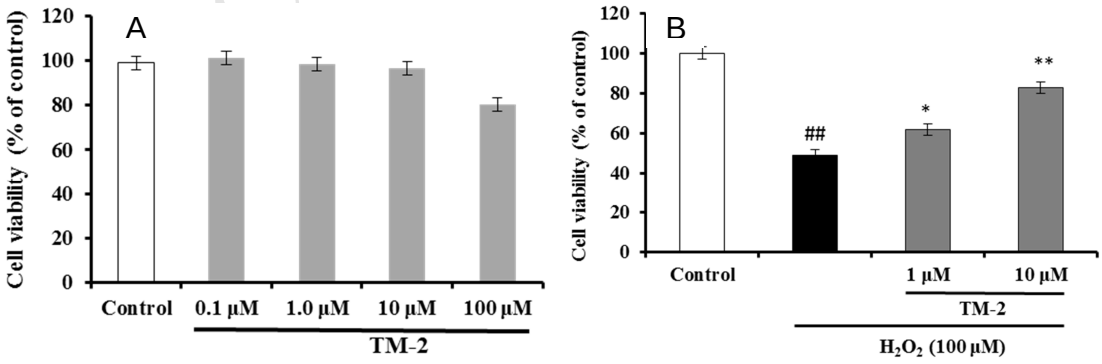

Figure 10 (A) Effects of **TM-2** on cell viability in PC12 cells. (B) Protective effects of **TM-2** on cell injury induced by H_2O_2 (100 μM) in PC12 cells. $^{\#\#}p < 0.01$ *vs* control; $^{*}p < 0.05$ *vs* H_2O_2 group and $^{**}p < 0.01$ *vs* H_2O_2 group.

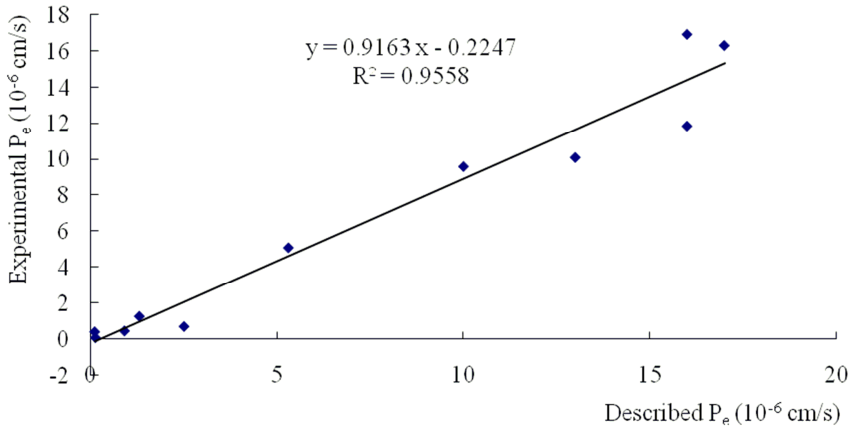

Figure 11 Lineal correlation between experimental and reported permeability of commercial drugs using the PAMPA-BBB assay. P_e(exp) = 0.9163P_e(bibl.) −0.2247 (R^2 = 0.9558).

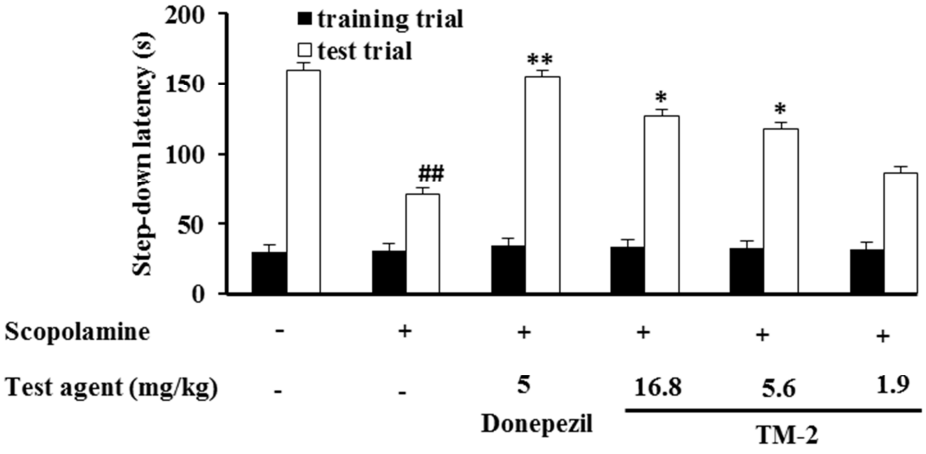

Figure 12 Effects of compound **TM-2** on scopolamine-induced memory deficit in the step-down passive avoidance test. Values are expressed as the mean ± SEM (n=10). # $p < 0.05$ *vs* normal group. * $p < 0.05$ and ** $p < 0.01$ *vs* scopolamine-treated control group.

Scheme 1. Synthesis of target compounds **TM-1~TM-5**. Reagents and conditions: (i) $Br(CH_2)_nBr$ (**2a~2d**), K_2CO_3, CH_3CN, 65 °C, 6-10 h; (ii) NHR_1R_2 (**4a~4b**), K_2CO_3, CH_3CN, refluxed, 6-8 h; (iii) 50% aqueous KOH, EtOH, room temperature, 3 to 4 days.

Scheme 2. Synthesis of target compounds **TM-6~TM-8**. Reagents and conditions: (i) $Br(CH_2)_nBr$ (**2a, 2b, 2d**), K_2CO_3, CH_3CN, 65 °C, 6-10 h; (ii) K_2CO_3, CH_3CN, refluxed, 6-8 h; (iii) 50% aqueous KOH, EtOH, room temperature, 3 to 4 days.

Scheme 3. Synthesis of target compound **TM-9**. Reagents and conditions: (i) Pd/C, H_2, EtOH, room temperature, 8h.

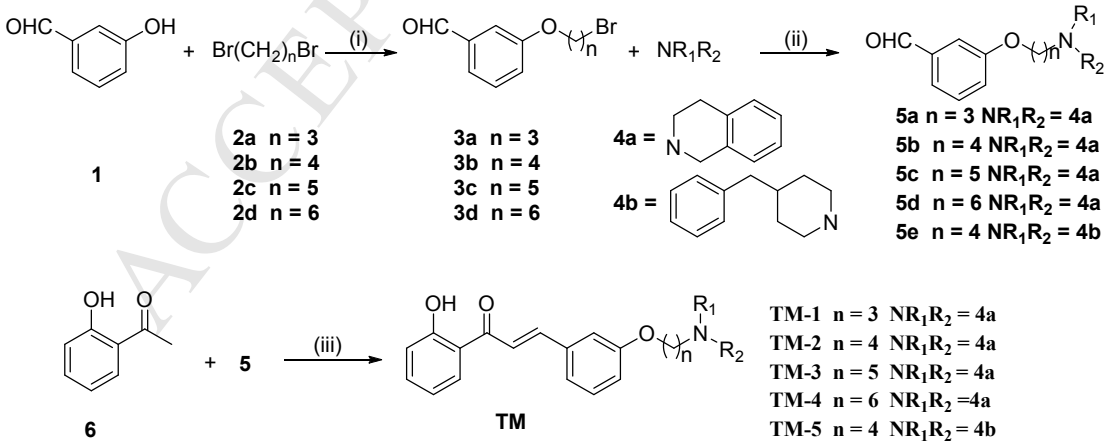

Scheme 1. Synthesis of target compounds **TM-1~TM-5**. Reagents and conditions: (i) $Br(CH_2)_nBr$ (**2a~2d**), K_2CO_3, CH_3CN, 65 °C, 6-10 h; (ii) NHR_1R_2 (**4a~4b**), K_2CO_3, CH_3CN, refluxed, 6-8 h; (iii) 50% aqueous KOH, EtOH, room temperature, 3 to 4 days.

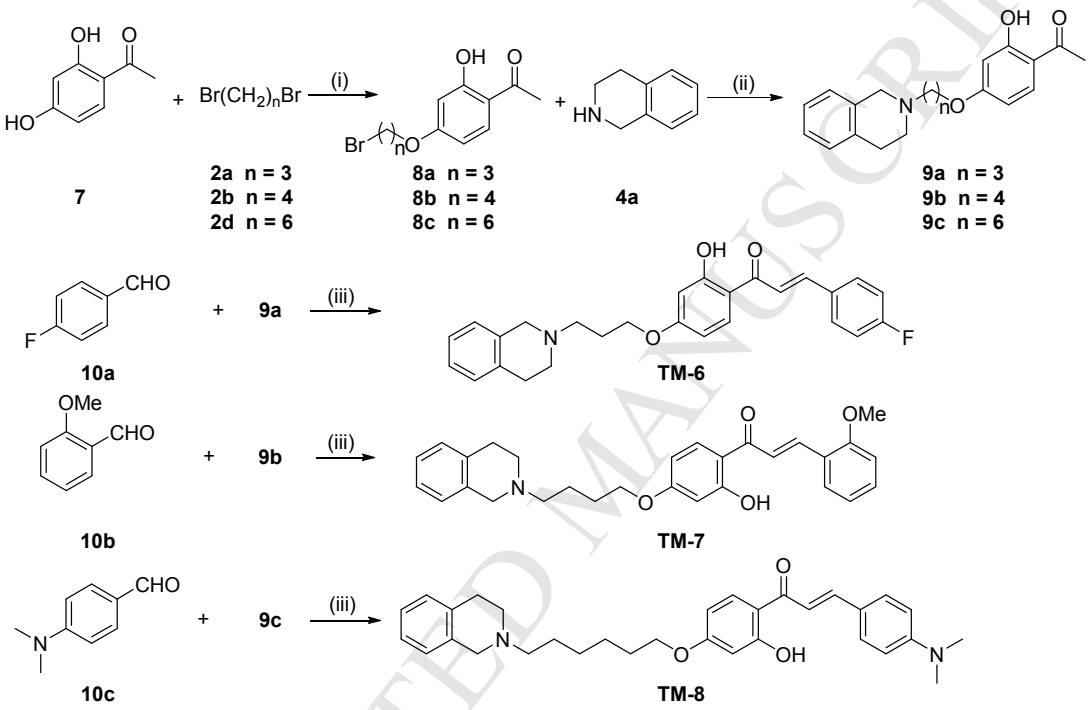

Scheme 2. Synthesis of target compounds **TM-6~TM-8**. Reagents and conditions: (i) $Br(CH_2)_nBr$ (**2a, 2b, 2d**), K_2CO_3, CH_3CN, 65 °C, 6-10 h; (ii) K_2CO_3, CH_3CN, refluxed, 6-8 h; (iii) 50% aqueous KOH, EtOH, room temperature, 3 to 4 days.

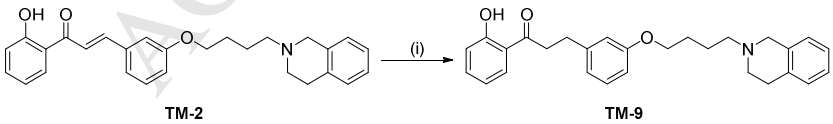

Scheme 3. Synthesis of target compound **TM-9**. Reagents and conditions: (i) Pd/C, H_2, EtOH, room temperature, 28h.

Table 1. Inhibition of AChE/BuChE and MAO-B/MAO-A, and their selectivity index by target compounds and referenced compounds.

Table 2. The antioxidant activity and effect on A$\beta_{1\text{-}42}$ aggregation of chalcone derivatives and referenced compounds.

Table 3 Permeability ($P_e \times 10^{-6}$ cm/s) in the PAMPA-BBB assay for 11 commercial drugs used in the experiment validation.

Table 4 Ranges of permeability of PAMPA-BBB assays ($P_e \times 10^{-6}$ cm/s)

Table 5 Permeability Pe ($\times 10^{-6}$ cm/s) in the PAMPA-BBB assay of compounds **TM-1~TM-9** and their predictive penetration in the CNS.

Table 6 Theoretical prediction of the ADME properties of compounds **TM-1~TM-9**

Table 1. Inhibition of AChE/BuChE and MAO-B/MAO-A, and their selectivity index by target compounds and referenced compounds.

Comp.	IC_{50} (μM) ± SD [a]		SI [d]	IC_{50} (μM) ± SD [a]		SI [g]
	*ee*AChE [b]	*eq*BuChE [c]		MAO-B [e]	MAO-A [f]	
TM-1	17.6±0.83	11.2±0.53	1.6	10.7 ± 0.27	29.8 ± 0.69	2.8
TM-2	16.2±0.34	2.6±0.03	6.2	5.3 ± 0.16	n.a. [h]	---
TM-3	18.6±0.22	3.7±0.05	7.2	4.8 ± 0.07	n.a. [h]	---
TM-4	27.1±0.97	4.1±0.02	6.6	6.7 ± 0.15	31.5 ± 0.47	4.7
TM-5	15.3±0.26	4.9±0.02	3.1	6.4 ± 0.31	n.a. [h]	---
TM-6	22.3±0.51	13.4±0.26	1.7	12.6 ± 0.46	26.1 ± 0.87	2.1
TM-7	8.3±0.03	5.2±0.01	1.6	9.5 ± 0.19	30.1 ± 0.05	2.4
TM-8	6.6±0.07	10.4±0.12	0.6	7.1 ± 0.08	n.a. [h]	---
TM-9	23.1±0.32	0.64±0.01	36	26.7 ± 0.39	n.a. [h]	---

Iproniazid	n.t. [i]	n.t. [i]		1.35 ± 0.02	5.48 ± 0.03	4.1
Rasagiline	n.t. [i]	n.t. [i]		0.0281±0.0068	0.587 ±0.038	20.9
Donepezil	0.019±0.0003	4.76±0.02	251	n.t. [i]	n.t. [i]	

[a] IC_{50} values represent the concentration of inhibitor required to decrease enzyme activity by 50% and are the mean of three independent experiments, each performed in triplicate (SD = standard deviation). [b] From *electrophorus electricus*. [c] *Eq*BuChE from *equine serum*. [d] SI = selectivity index = IC_{50} (BuChE)/IC_{50} (AChE). [e] From recombinant human MAO-B. [f] From recombinant human MAO-A. [g] hMAO-B selectivity index = IC_{50} (MAO-A)/IC_{50} (MAO-B). [h] n.a. = no active, representing MAO-A/MAO-B inhibition rate of compounds < 5% at 10 μM. [i] n.t. = not tested.

Table 2. The antioxidant activity and effect on A$\beta_{1\text{-}42}$ aggregation of chalcone derivatives and referenced compounds.

Compound	ORAC[a]	Effect on of A$\beta_{1\text{-}42}$ aggregation (%)[b]		
		Inhibit self-induced [c]	Inhibit Cu^{2+}-induced [d]	Disaggregate Cu^{2+}-induced [e]
TM-1	1.1±0.02	65.9 ± 0.76	n.t. [f]	n.t. [f]
TM-2	1.2±0.02	70.2 ± 0.38	80.7 ± 0.29	73.5 ± 0.24
TM-3	1.2± 0.01	69.7 ± 0.32	n.t. [f]	n.t. [f]
TM-4	1.1± 0.01	65.6 ± 0.61	n.t. [f]	n.t. [f]
TM-5	1.2± 0.01	71.4± 0.22	n.t. [f]	n.t. [f]
TM-6	0.92±0.01	72.4 ±0.38	n.t. [f]	n.t. [f]
TM-7	1.5± 0.01	83.1±0.52	n.t. [f]	n.t. [f]
TM-8	1.6± 0.01	97.5 ±0.46	n.t. [f]	n.t. [f]
TM-9	1.4± 0.02	n.t. [f]	n.t. [f]	n.t. [f]
Curcumin	n.t. [f]	47.3 ± 0.01	76.5 ± 0.02	56.5± 0.21
Donepezil	n.t. [f]	n.a. [g]	n.t. [f]	n.t. [f]

[a] Results are expressed as μM of Trolox equivalent/μM of tested compounds. [b] Inhibition of A$\beta_{1\text{-}42}$ aggregation and disaggregation of A$\beta_{1\text{-}42}$ aggregation, the thioflavin-T fluorescence method was used, data are the mean ± SEM of three independent experiments. [c] Inhibition of self-Induced A$\beta_{1\text{-}42}$ aggregation, the concentration of tested compounds and A$\beta_{1\text{-}42}$ were 25 μM. [d] Inhibition of Cu^{2+}-induced A$\beta_{1\text{-}42}$ aggregation. The concentration of tested compounds and Cu^{2+} both were 25 μM. [e] Disaggregating of Cu^{2+}-induced A$\beta_{1\text{-}42}$ aggregation, the concentration of tested compounds and A$\beta_{1\text{-}42}$ were 25 μM. [f] n.t. = not tested. [g] n.a. = no active. Compounds defined "no active" means percent inhibition less than 5.0% at a concentration of 25 μM.

Table 3 Permeability ($P_e \times 10^{-6}$ cm/s) in the PAMPA-BBB assay for 11 commercial drugs used in the experiment validation.

Commercial drugs	Bibl [a]	PBS:EtOH(70:30) [b]
verapamil	16	16.9
oxazepam	10	9.6
diazepam	16	11.86
clonidine	5.3	5.1
Imipramine	13	10.1

testosterone	17	16.3
caffeine	1.3	1.28
enoxacine	0.9	0.471
piroxicam	2.5	0.718
norfloxacin	0.1	0.423
theophylline	0.12	0.1

[a] Taken from ref [35].

[b] Data are the mean ± SD of three independent experiments

Table 4 Ranges of permeability of PAMPA-BBB assays ($P_e \times 10^{-6}$ cm/s)

Compounds of high BBB permeation (CNS+)	$P_e > 3.44$
Compounds of uncertain BBB permeation (CNS+/-)	$3.44 > P_e > 1.61$
Compounds of low BBB permeation (CNS-)	$P_e < 1.61$

Table 5 Permeability Pe ($\times 10^{-6}$ cm/s) in the PAMPA-BBB assay of compounds **TM-1~TM-9** and their predictive penetration in the CNS.

compound[a]	Pe ($\times 10^{-6}$ cm/s)[b]	prediction
TM-1	10.18 ± 0.63	CNS+
TM-2	11.34 ± 0.29	CNS+
TM-3	10.02 ± 0.49	CNS+
TM-4	11.85 ± 0.59	CNS+
TM-5	12.35 ± 0.54	CNS+
TM-6	12.56 ± 0.77	CNS+
TM-7	13.11 ± 0.67	CNS+
TM-8	13.16 ± 0.38	CNS+
TM-9	16.79 ± 0.93	CNS+

[a] Compounds **TM-1~TM-9** were dissolved in DMSO at 5 mg/mL and diluted with PBS/EtOH (70:30). The final concentration of compounds was 100 μg/mL.

[b] Values are expressed as the mean ± SD of three independent experiments.

Table 6 Theoretical prediction of the ADME properties of compounds **TM-1~TM-9**

Comp.	miLog *P*	pKa	MW	TPSA (Å^2)	n-ON	n-OHNH	volume (Å^3)
TM-1	5.48	7.943	413.5	49.77	4	1	393.02
TM-2	5.77	7.943	427.5	49.77	4	1	409.82
TM-3	6.25	7.943	441.6	49.77	4	1	426.62
TM-4	6.76	7.943	455.6	49.77	4	1	443.42
TM-5	6.93	7.943	469.6	49.77	4	1	460.25
TM-6	5.64	7.530	431.5	49.77	4	1	397.95
TM-7	5.58	7.543	457.6	59.01	5	1	435.36
TM-8	6.86	7.725	498.7	53.01	5	1	489.33
TM-9	5.72	8.535	429.6	49.77	4	1	416

[a] MW, Molecular weight; TPSA, topological polar surface area; n-OH, number of hydrogen acceptors; n-OHNH, number of hydrogen bond donors. The data were determined with the Molinspiration calculation software.

Highlights.

- Compound **TM-2** was a selective BuChE inhibitor (IC_{50} = 2.6 μM) and selective MAO-B inhibitor (IC_{50} = 5.3 μM)
- Compound **TM-2** showed good antioxidant activity and served as neuroprotectant
- Compound **TM-2** was a selective metal chelator, and could significantly inhibit/disaggregate self-induced and Cu^{2+}-induced A$\beta_{1\text{-}42}$ aggregation.
- Compound **TM-2** was a potent selective MAO-B inhibitor.
- Compound **TM-2** displayed good PAMPA-BBB permeability and conformed to the Lipinski's rule.
- Compound **TM-2** presented precognitive effect on scopolamine-induced memory impairment